Thorium Oxide Dissolution Kinetics for Hydroxide and Carbonate Complexation

by

Virginia Curran

SB, Nuclear Engineering

Massachusetts Institute of Technology (1999)

Submitted to the Department of Nuclear Engineering
in Partial Fulfillment of the Requirements for the Degree of
Master of Science in Nuclear Engineering

At the

Massachusetts Institute of Technology

June 2001

Signature of Author.....
Department of Nuclear Engineering
May 11, 2001

Certified by.....
Kenneth R. Czerwinski
Assistant Professor of Nuclear Engineering
Thesis Supervisor

Certified by.....
Mujid S. Kazimi
Professor of Nuclear Engineering
Thesis Reader

Accepted by.....
Sow-Hsin Chen
Chairman, Graduate Thesis Committee

Thorium Oxide Dissolution Kinetics
for Hydroxide and Carbonate Complexation

by

Virginia Curran

Submitted to the Department of Nuclear Engineering
on 11 May, 2001 in Partial Fulfillment of the Requirements
for the Degree of Master of Science in Nuclear Engineering

Abstract

In order to better understand the behavior of thorium breeder reactor fuel in a repository environment, the behavior of thorium oxide was investigated. The kinetics of crystalline thorium oxide dissolution were studied under argon and argon/10% CO_2 over a broad pH range in 0.1 M ionic strength $NaClO_4$ solution. Samples were analyzed for thorium concentration using ICP-AES, ICP-MS, and NAA. Data was fit to a first order kinetics model. The kinetic rate constant under pure argon was 0.0107 ± 0.00123 h^{-1} for pH 2-3. Under 10% CO_2, the rate constant was 0.00511 ± 0.000863 h^{-1}. No kinetics results could be discerned from the data at higher pH. Under argon, solubility at pH greater than 3 was at nm/L levels, three orders of magnitude lower than at pH 3 and below. Under 10% CO_2, solubilities decreased from 10 μmol/L at pH 2.06 to 80 nm/L at pH 3.

Thorium oxide powder remnants from each experiment were analysed using XRD, FTIR, and BET surface area analysis. Surface area analysis showed a 15% increase in surface area at pH 10 and higher under argon, and a uniform surface area increase of 15 to 30% under 10% CO_2. XRD and FTIR spectra showed that the thorium oxide was otherwise identical to the untreated standards.

Thesis Supervisor: Ken Czerwinski
Title: Assistant Professor, Nuclear Engineering

Thesis Reader: Mujid Kazimi
Title: Professor, Nuclear Engineering

Acknowledgements

First, thanks to all of the people who helped me out, whether I needed it or not. To my advisor, the groovy Ken, thanks for the great "why do you want to write a master's thesis" encouragement. To Jianmei, for counting my samples, albeit on your own schedule. It really is possible to do 70 in one week, see? To Professor Kazimi, for the wonderful thorium group meetings that truly encouraged me to finish this work as quickly as humanely possible. To Pat Allen, for showing me the way. To Gentech Scientific and the anonymous pharmaceutical company, just for having the ICP-MS that I am eagerly awaiting. To Wendy and Yoann, for stealing and eventually freeing me from that ceramics business. And especially thanks to my French thorium kidnappers, I mean colleagues, for the ever so timely sample analysis, and for convincing Ken in a rather roundabout fashion that we need our own ICP-MS. I'd like to especially thank Florence Goutelard of CEA Saclay, Paris for all her toils with the ICP-MS and my excessive sodium.

Secondly, I would like to thank all of the wonderful people who make MIT such a fun and interesting place. To Randi, the most awesome friend a person can have and a well known bacteria murderer. Good luck at med school. To Leigh, the Red Sox biggest fan. To all of the secretaries and support staff, who are always there in a pinch when I need help at the last minute. To Brian, someday we'll make it to Goth night. I swear. To LSC, because you suck and always will. To Chuck Vest, for having no backbone. And to all those anonymous administrators and their two hour lunch breaks. I aspire to be you some day.

Finally, I'd like to thank my wonderful yet obnoxious husband for all of his support, no matter how masked it may have been. Yeah, I'm gonna be your sugar momma. Here's to 2003.

I dedicate this wonderful work of art to my parents, who have always loved and accepted me even though I was quite a bit different from the rest. Some day I hope I can show you the world.

Table of Contents

List of Figures

List of Tables

Chapter 1: Introduction

There has been a recent resurgence of interest in thorium as a potential advanced fuel for Generation IV nuclear energy systems that can be operated to relatively high burnups at lower costs than current UO_2 fuels. In addition, it is thought that ThO_2-UO_2 fuels will be less expensive to fabricate than uranium dioxide (UO_2) fuel, allow higher sustainable plant capacity factors, result in a more stable and insoluble waste form, be very resistant to weapons-material proliferation, and reduce the federal government's costs for spent fuel disposal [1]. Because there is a likelihood that a thorium based fuel cycle will be implemented in commercial nuclear power reactors in the future, it is important to study the behavior of such fuel in the environment. To date, very few experimental studies have been performed.

The purpose of this project was to determine the kinetics and thermodynamics of thorium oxide dissolution in the environment. Solubility is the concentration of the soluble form of an element in an aqueous solution at equilibrium. It is a function of temperature and the components in the system [2]. The rate at which equilibrium is reached is controlled by kinetics processes, meaning the rate at which solution reaches equilibrium varies based on the solution. Solubility is important because it establishes an upper concentration limit on the concentration of a dissolved radionuclide in solution [3].

While understanding the behavior of thorium fuels in the proposed repository at Yucca Mountain is most applicable, a more rigorous study of thorium solubility over a wide pH range was performed so that the data could also be used to model the behavior of thorium fuels in any environmental system. To achieve this, the kinetics and thermodynamics of thorium oxide dissolution under both pure argon and argon with pCO_2 of 0.1 were studied

under the full pH range available in each atmosphere. In addition, thorium oxide powder remnants were studied after each experiment to examine structural changes that may affect kinetics.

1.1 Experiment overview

The kinetics and thermodynamics of thorium oxide dissolution were studied under two atmospheres. A pure argon atmosphere was used to examine the formation of the hydroxide species, and a mixture of 90% argon and 10% CO_2 was used as the cover gas when studying carbonate complexation. Thorium oxide powder was placed in a pH adjusted solution of 0.1 M ionic strength and allowed to dissolve over a period of one month. For the experiments under argon, the pH ranged from 2 through 12 in steps of 0.5. Under the argon/CO_2 mixture, the pH range was limited to 2 through 6.5 due to strong carbonate buffering. Steps were also of 0.5 pH.

Filtered samples were taken every three days for the kinetics data. In addition, with every third sample, an unfiltered sample was also taken in order to determine if any colloids greater than the filter size of 0.2 μm were forming. Colloids are small particles composed of either single large molecules or clusters of smaller molecules which range in size from 0.001 to 1 μm. Since the presence of colloids could affect reaction kinetics, it is important to determine if any are being formed. In addition, mobile colloids in significant concentrations can increase migration of radionuclides through groundwater [2].

Samples of sufficient concentration were analyzed using a Spectroflame ICP-AES. Lower concentration samples were either analyzed using an ICP-MS or by neutron activation analysis.

Chapter 2: Background

Due to the resurgence of interest in the thorium fuel cycle, a project is underway in conjunction with MIT and INEEL to design a thorium based fuel from the perspective of the final waste disposition. A zirconia based fuel design was chosen due to the high stability of the cubic fluorite zirconia structure. In order to properly model the behavior of the zirconia-based ceramic fuel in a repository environment, it is important to understand the solubility of ThO_2 on a fundamental level.

2.1 Thorium Breeder Reactor

A thorium breeder reactor is a light water reactor that uses uranium-thorium fuel. The uranium provides the fissile seed fuel, while the thorium (initially all ^{232}Th) is the fertile blanket. While in the neutron flux, the ^{232}Th absorbs a neutron, becoming ^{233}Th. After two β decays and a half-life of about a month, the ^{233}Th turns into ^{233}U, a fissile fuel that produces more neutrons per reaction than ^{235}U, the industry standard fissile fuel. This is shown in figure 2.1. Thorium breeder reactors have the potential to increase the length of the fuel cycle, since new fissile fuel is building into the core as the original fissile content is burned up. In addition, a thorium breeder core can be designed for direct use in current nuclear power reactor designs.

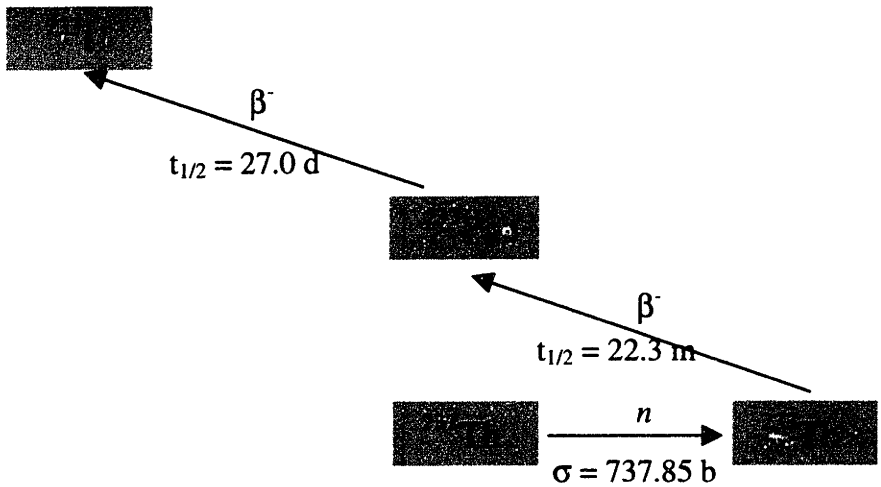

Figure 2.1 ^{233}U production

2.2 Ceramic fuel solubility

A zirconia (ZrO_2) based fuel form was chosen because it is known to be both chemically stable and radiation resistant [4], and has a very low thermal neutron capture cross section, around 0.2 b [5]. Studies have shown that zirconia is more radiation resistant than both pyrochlore ($Gd_2Ti_2O_7$) and zirconalite ($CaZrTi_2O_7$) ceramics, which are to be used as the host phase for weapons grade plutonium immobilization [4,6]. In addition, zirconia shares its face centered cubic fluorite-type structure with ThO_2 (thoria) and UO_2 (urania), making it ideal for combination with the thoria and urania phases [7]. The natural analogue of zirconia, baddeleyite ($(Zr,M)O_2$, where M is a metal such as hafnium), contains up to 3000 ppm uranium or thorium [8]. Negligible or no loss of lead, a stable decay product of uranium and thorium, in natural baddeleyites indicates high chemical durability [4].

Various zirconia ceramics have been fabricated and studied, including ZrO_2-PuO_2, ZrO_2-UO_2, ZrO_2-ThO_2, and ZrO_2-CeO_2 [4], and there is a lot of information on fabrication

and behavior of UO_2-ThO_2 ceramics [7,9]. Ceramics that have been fabricated frequently contain a small amount of Y_2O_3 (up to 15 mol% [4]) binder in order to stabilize the ceramic. All of these ceramic compositions have shown superior durability to their zirconia free counterparts [4,6,7,9], though there have been problems with urania-thoria phase separations, though the inclusion of Zr in the lattice tends to strengthen the bonding [7]. No studies have been performed on these ceramics under neutron irradiation, though there is ample data on heavy ion bombardment of zirconalite and zirconia [4,6].

Currently there is no published data on combined $(Zr,Th,U)O_2$ ceramics. Preliminary work has been undertaken at MIT to investigate these ceramics. MgO has been used as a binder for the fuel, since the ZrO_2-Y_2O_3 structure is known to break down at temperatures above 500 °C [10]. Analysis has shown that the MgO binder (0.5 wt%) increases both strength and density [11].

The stability and solubility of the fuel (and eventual waste form) has not been studied very extensively. While there have been some studies on the solubility of unirradiated ThO_2 [12-16,18,20,21] and a few more on unirradiated $(Th,U)O_2$ under various conditions [13,17,19], the data varies widely, and the majority consider artificial environments such as acids [13-15,17,18] or other media [12,15]. According to Sunder and Miller [19], dissolution of uranium from $(Th,U)O_2$ is much lower than that from UO_2 fuel under similar conditions. ThO_2 dissolution has also been shown to be fairly low, though most tests were either performed under artificial conditions or over a limited pH range [20]. Zirconia has also been shown to have very low solubility, less than 0.1 nmol/L, with very little variation with temperature [22]. Leach tests that have been performed on zirconalites [6] and some zirconia ceramics [4] show favorable results, however no dissolution or leach rate tests on

(Zr,Th,U)O2 ceramics have been published to date. No data concerning solubility of irradiated thoria fuels was found, though leach tests on thoria ceramics containing lanthanum as a simulated fission product were performed, with favorable results [23].

2.3 Thorium Oxide Dissolution

While the solubility of thorium oxide has been studied sporadically over the past forty years, little work has been done on the kinetics of dissolution. Because of this, many studies were performed over insufficient time periods to achieve equilibrium. Most kinetics studies that have been performed were in mixtures of nitric and hydrofluoric acid [24-26], systems useful for dissolving thorium bearing ore. Because of the high concentration of fluoride and H^+, the acids do not resemble natural waters and the results are therefore not useful for determining kinetics and thermodynamics in natural systems.

Carbonate complexation has been shown to be important for many metal ions [27], though there have been very few studies on the effects of the carbonate and bicarbonate ligands on kinetics. A study by Östhols and Malmström showed that while carbonate complexation can have a marked effect on kinetics, bicarbonate complexation does not [28]. This study was performed over a very limited and acidic pH range and therefore may not correspond to natural systems. In addition, it has not yet been verified by anyone else.

2.4 Thoria Behavior in Aqueous Systems

The thorium aqueous phase consists of three parts: the free thorium (Th^{4+}), thorium hydroxide species, and thorium carbonate species, as expressed by

$$[Th]_{aq} = [Th^{4+}] + \sum_{x=1}^{4} [Th(OH)_x^{4-x}] + \sum_{y=1}^{4} [Th(CO_3)_y^{4-2y}]$$

In order to determine the concentration of species in a particular environment, solubility and stability constants are needed. The formation of the free species can be described by the hydrolysis reaction

$$ThO_2 + 2H_2O \Leftrightarrow Th^{4+} + 4OH^-$$

and the solubility product constant, K_{sp}, is given by

$$K_{sp} = [Th^{4+}][OH^-]^4$$

For the hydroxide and carbonate species, the formation is described by

$$Th^{4+} + aL^{-z} \Leftrightarrow ThL_a^{4-az}$$

Where L is either OH^- or CO_3^{2-} (depending on the species), and the equation for the stability constant is

$$\beta_{ThL_a} = \frac{[ThL_a^{4-az}]}{[Th^{4+}][L^{-z}]^a}$$

At any given pH, the concentration of the free species is determined by the solubility product constant, the concentration of the hydroxide species is determined from the pH, and the carbonate species concentration is determined from both the pH and the CO_2 partial pressure.

Due to buffering by the carbonate system, the maximum attainable stable pH of a system under CO_2 is limited. This limit is dependant on the partial pressure of the CO_2 cover gas. The carbonate concentration of a system under high CO_2 partial pressure and low pH can be

extrapolated to a corresponding system under lower CO_2 partial pressure and a higher pH using the following equation [29]:

$$\log[CO_3^{2-}] = -17.55 \pm 0.09 + 2\text{pH} + \log pCO_2$$

With this information, the stability constants can be calculated and the total thorium concentration under those conditions can be determined from the equation:

$$[\text{Th}]_{aq} = [\text{Th}^{4+}] + \sum_{x=1}^{4} \beta_{\text{Th(OH)}_x} [\text{Th}^{4+}][\text{OH}^-]^x + \sum_{y=1}^{4} \beta_{\text{Th(CO}_3)_y} [\text{Th}^{4+}][CO_3^{2-}]^y$$

Figure 2.1 shows an initial estimate of the solubility of thorium over a range of pH (3 through 10). Higher solubility at low and high pH is expected, with a minimum in between. The pH range of Yucca Mountain (6.7 to 9.3) is expected to lie in the minima. Data for this graph is from a combination of values from the literature and estimates [30].

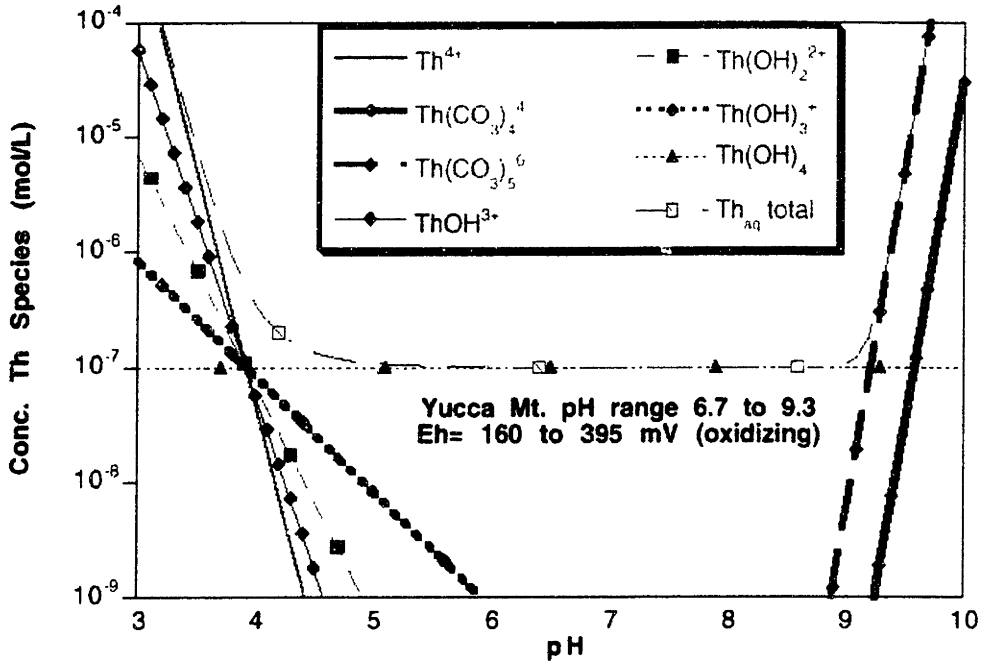

Figure 2.2: Thorium Solubility Estimate

Chapter 3: Experimental Methods

3.1 Solubility Experiment Setup

Solubility experiments were run under both pure argon gas and a mixture of argon/10% CO_2. The gas was passed through a water or mineral oil bubbler before reaching the seven 100 mL three necked round-bottomed flasks, which were set up in series (Figure 2.1). Each flask was filled with 90 mL of 0.1 M $NaClO_4$. Flasks were adjusted to pH 2 through 12 in 9.5 pH steps under argon and pH 2 through 6.5 under the argon/10% CO_2 mixture due to strong buffering at pH 6.5. 0.1 M $HClO_4$ was added to lower pH and 0.1 M NaOH was added to increase pH.

Figure 3.1 Solubility experiment setup

Flasks were allowed to equilibrate under the prescribed atmosphere for at least one hour before addition of thorium oxide. Approximately 1 g of crystalline ThO_2 was added to each flask after atmospheric equilibration. The excess ThO_2 was added to ensure that there would be enough for the various analyses, such as BET surface area measurements and x-ray diffraction, which were to be performed after each experiment.

Flask pH was measured with a Corning liquid KCl (argon, pH 2-6) or gel electrolyte filled pH probe calibrated daily at pH 4, 7, and 10 and checked at least monthly over the full pH range (pH 2 through 12.45) with fresh buffers. The pH of each flask was checked and adjusted at least once per day. While it was fairly difficult to maintain pH under pure argon at higher pH (6 and up), pH under argon/10% CO2 remained fairly constant with minimal adjustments throughout the experiment. Table 3.1 shows the average pH for each flask in the experiment.

Flask	pH	Atmosphere	Flask	pH	Atmosphere	Flask	pH	Atmosphere
1	2.07	Ar	13	8.96	Ar	25	3.60	Ar/10%CO_2
2	2.57	Ar	14	9.52	Ar	26	4.13	Ar/10%CO_2
3	2.99	Ar	15	10.07	Ar	27	4.48	Ar/10%CO_2
4	3.68	Ar	16	10.6	Ar	28	5.05	Ar/10%CO_2
5	4.27	Ar	17	11.08	Ar	29	5.51	Ar/10%CO_2
6	5.24	Ar	18	11.55	Ar	30	6.03	Ar/10%CO_2
7	5.84	Ar	19	12.04	Ar	31	6.38	Ar/10%CO_2
8	6.40	Ar	20	4.27	Ar	32	6.48	Ar/10%CO_2
9	6.90	Ar	21	5.45	Ar	33	3.00	Ar/10%CO_2
10	7.38	Ar	22	2.06	Ar/10%CO_2	34	4.03	Ar/10%CO_2
11	8.08	Ar	23	2.57	Ar/10%CO_2	35	4.96	Ar/10%CO_2
12	8.6	Ar	24	3.1	Ar/10%CO_2			

Table 3.1 Flask pH and atmosphere

3.2 Sampling Procedure

Flask pH was monitored daily to ensure that it remained relatively stable over the course of each experiment. On every third day, a 4.0 mL sample was pipetted into a 10 mL B&D

sterile syringe and filtered through a 0.2 μm Acrodisc syringe filter. From the initial sample, 3.5 mL was transferred into a 15 mL polypropylene centrifuge tube. 23 μL of reagent grade 15.56 M nitric acid was added to each sample to bring the samples to a 0.1 M nitric acid concentration. Afterwards, the samples were mixed with a vortex and placed in a refrigerator for storage. For every third sample set, a 3.5 mL unfiltered sample was also taken in order to determine if any large (greater than 0.2 μm colloids) were being formed. This sample was directly pipetted into the 15 mL centrifuge tube. Sample preparation was otherwise identical to the filtered samples.

In order to have enough sample volume to try several different analysis methods, a 5.0 mL volume was initially removed and filtered from each flask from the last sets of samples (pH 5.5 through 6.5 under 10% CO_2). 4.5 mL was then transferred to a 15 mL centrifuge tube, and 30 μL of 15.56 M nitric was added. Unfiltered samples started with 4.5 mL directly pipetted to the centrifuge tubes. Unfiltered sample preparation was otherwise the same. All samples were mixed with a Vortex and stored in a refrigerator until analysis could be performed.

3.3 ICP-AES Procedure

Samples with dissolved thorium concentrations around 0.1 through 10 μmol/L were analyzed using inductively coupled plasma atomic emission spectroscopy, ICP-AES. For the ICP-AES method, the liquid samples were fed directly as prepared into the instrument for analysis.

For this experiment, the samples were analyzed using the 401.913 nm emission line. All samples were diluted to 0.1 M HNO_3 in order to minimize sorption of thorium to surfaces such as polypropylene tubes and quartz glass.

3.3.1 Principle of ICP-AES

The principle behind ICP-AES is that a plasma is generated by an igniting device consisting of an oscillating electromagnetic field established by a high frequency coil wrapped around a quartz torch. The oscillating field causes argon atoms to collide, transferring energy to other argon atoms, which become ionized and cause further collisions. This process continues until the plasma reaches a steady state. Aqueous samples are introduced into the system via a peristaltic pump, which pumps the sample through a nebulizer. The nebulizer creates a fine aerosol mist. Particles that are small enough to be excited by the plasma are carried away by argon gas into the plasma. Once in the plasma, sample atoms collide with the rapidly moving plasma atoms and become excited. These excited atoms eventually relax to a lower energy state and emit characteristic photons. A spectrometer, set to measure a specific characteristic energy, measures the intensity of the emitted photons [31]. Figure 3.2 shows the basic arrangement of an ICP-AES. The operation of the plasma torch is depicted in Figure 3.3.

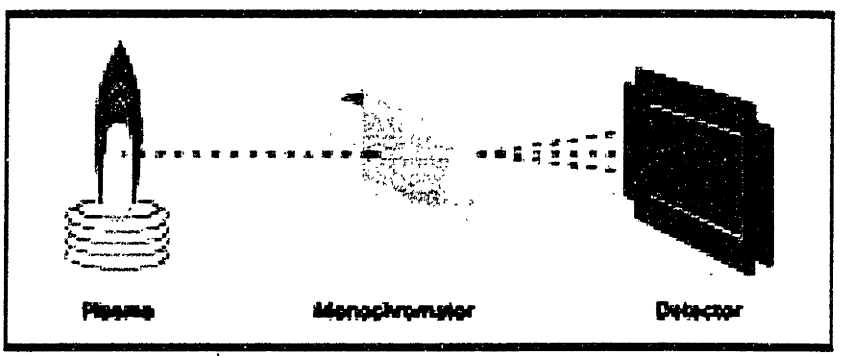

Figure 3.2 ICP-AES basic arrangement

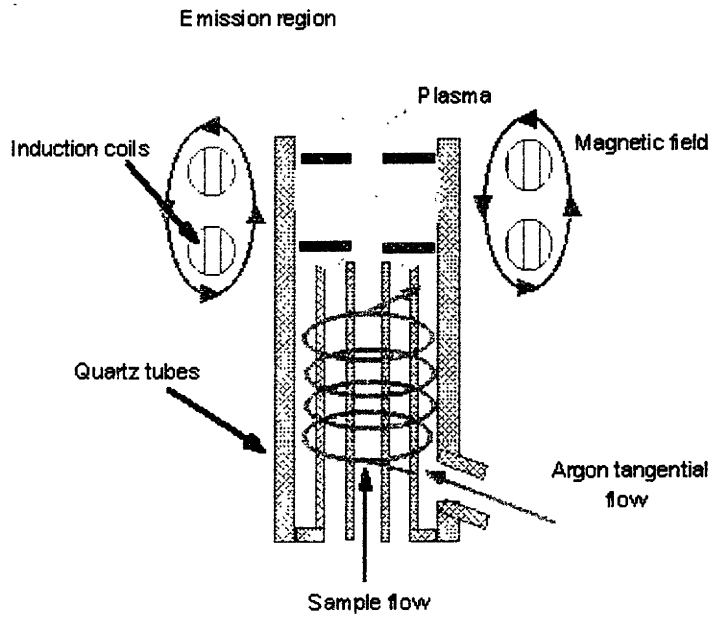

Figure 3.3 ICP-AES plasma torch operation

This sample analysis technique cannot tell an absolute concentration due to uncertainties in the nebulizer efficiency, optical efficiency, and other aspects of the system. A relative concentration can be determined by calibrating the system each time with known standards in order to determine the concentration in the samples. Standard concentrations can range from the lower detection limit to just below the saturation point of the machine. A linear regression fit of the data from the standards is then used to determine the concentration of each unknown sample.

The best way to lower the detection limit of the system is to increase the efficiency of the nebulizer. A standard pneumatic nebulizer has an efficiency of around 1%-3%, while an ultrasonic nebulizer can have an efficiency as much as 15 times as high. In addition, samples should be slightly acidified in order to minimize sorption to the surface of tubes and glassware

in the instrument, which can increase the background and therefore the detection limit of the machine.

3.3.2 Standard Preparation

The method of standard preparation and type of standard used for ICP-AES calibration can affect the quality of the data and is therefore very important. The most important aspect of standard preparation is to match the standard matrix to the sample matrix. This is to account for any interferences the matrix may cause with the optical line of interest. In order to account for any optical interference that the bright orange flame created by sodium in the torch may cause, all standards were prepared in a 0.1 M $NaClO_4$ solution matching that of the samples. It is also important to create a large enough range of standards to cover the expected range of sample concentrations, so that a good calibration curve can be created in the correct region. This is especially important when determining concentrations near the detection limit of the instrument, since most curve fitting programs will preferentially weight the curve to the higher concentration data.

Initial analysis showed that sample concentrations ranged from below the detection limit of the instrument to approximately 10 µmol/L. Standards were prepared ranging from 0.1 µmol/L to 100 µmol/L by diluting Aldrich 970 µg/L (4.18 mmol/L) thorium atomic absorption standard solution with 0.1 M $NaClO_4$ to match the sample matrix. The standards were then diluted to 0.1 M HNO_3 using the appropriate amount of 15.56 M reagent grade nitric acid, also to match the sample matrix, as well as to limit sample plating in the poly lines and glassware. In addition, a 10 nmol/L standard was prepared in the same manner and used as a "matrix blank" in order to determine the background count rate of the instrument. This

standard was chosen because it was well below the detection limit of the machine, consisted of the same matrix as the samples and the standards, and there was sufficient volume left over from neutron activation analysis standard preparation for use in this manner.

3.3.3 Procedure

The standard startup procedure for the Spectro Analytical Instruments Spectroflame ICP-AES was followed each time the instrument was used. A minimum warm-up time of 15 minutes was allowed while flushing the instrument with purified water at each startup. The sequential optics were then reprofiled in order to accommodate any changes in instrument operation parameters since the last use. Two thorium emission lines were available for use. The sample analysis method was set up to look at both lines simultaneously, but the 401.913 nm line was always preferentially used for data analysis due to its larger intensity and lower detection limit. The 283.730 nm line was mainly used to check that the ICP-AES was working properly. After reprofiling the optics, the location of the actual thorium peak was checked against the machine determined location using the strongest standard in order to assure that the optics were properly calibrated. The location of the thorium peaks did not move at any time.

The instrument was flushed with 5 vol% nitric acid after the peak location check in order to remove any lingering thorium from the system. The background was then checked against the initial background to ensure that the system was clean. All poly tubes were replaced periodically to ensure the data was not affected by thorium plating on the tubing. In addition, the spray chamber and torch were cleaned by soaking in a 5 vol% hydrochloric acid bath for several hours followed by a thorough rinsing in purified water every month.

Once the lines were sufficiently clean, the thorium standards were run in order of increasing concentration to create a calibration curve. A matrix background was taken before the first (lowest concentration) standard. After the final (highest concentration) standard was analyzed, the system was again flushed with 5 vol% nitric acid until the background returned to the initial level. This was double checked by running another matrix background for comparison to the previous one. Samples were then run in order of lowest estimated concentration to highest. A two minute 5 vol% nitric flush was performed between each sample in order to limit plating. Nitric backgrounds were taken periodically for comparison. Every ten samples, a blank matrix background was taken to further ensure that sorption of thorium to the instrument surfaces was not interfering with the data.

Following each ICP use, the instrument was shut down using the Spectro procedure. The instrument was flushed with purified water for a minimum of ten minutes before the torch was turned off. The system was then allowed to cool for another five to ten minutes and then turned off.

3.4 ICP-MS Procedure

Samples from the pure argon atmosphere experiments that were below the detection limit of the ICP-AES system were analyzed using a quadropole ICP-MS system at L'aboratoire d'Analyse Isotopique et Elémentaire at the Commisserat à L'Energie Atomique (CEA) in Paris, France.

3.4.1 Principles of ICP-MS

In plasma mass spectroscopy, the inductively-coupled argon plasma (ICP) is once again used as an excitation source for the elements of interest. However, in contrast to plasma emission spectroscopy, the plasma in ICP-MS is used to generate ions which are then introduced to the mass spectrometer and focused by a cone. These ions are then separated by the a lens (ion separator). The ions change trajectory when they enter the quadropole magnetic field (mass filter), and are collected according to their mass to charge ratios in electron multiplier cup detectors. The constituents of the unknown sample can then be identified and measured by the detectors. ICP-MS offers extremely high sensitivity for many elements and can also be successfully applied to a wide range of elements. Figure 3.4 shows the basic components of an ICP-MS system. Detection limits of ICP-MS systems can be from one to four orders of magnitude lower or more than their ICP-AES counterparts.

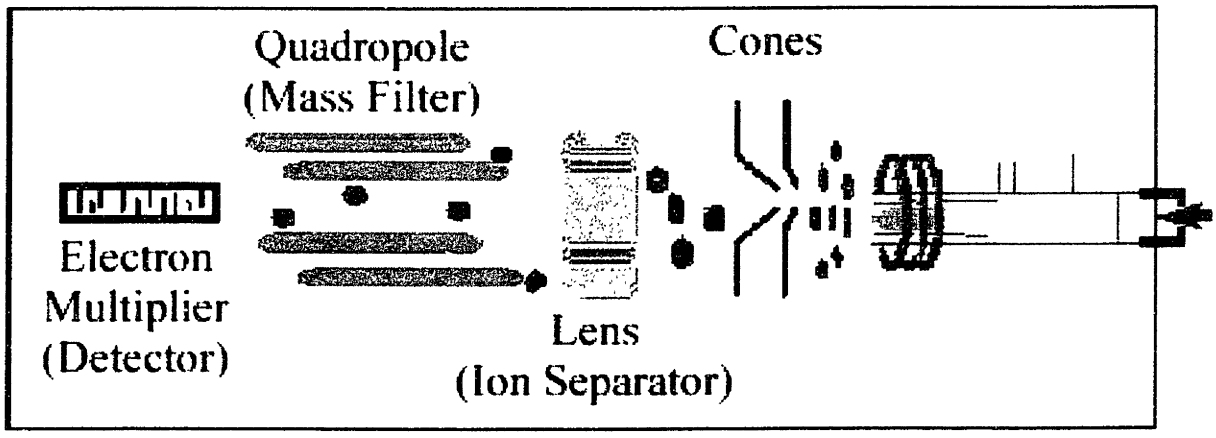

Figure 3.4 Major Components of an ICP-MS

Like ICP-AES, the ICP-MS technique is used to determine relative concentrations. Known standards must be use to calibrate the ICP data and determine actual concentrations.

3.4.2 Sample preparation

ICP-MS analysis was performed at CEA Saclay in Paris, France. Samples were sent as prepared for ICP-AES to France to be analyzed. Due to difficulties with high sodium content, which induced instabilities in the thorium signal. Studies with $NaClO_4$ showed that the maximum allowable concentration before instabilities occurred was 0.02 M. Therefore, all samples were diluted by a factor of 5 with purified water in order to minimize system instabilities.

3.4.3 Standard preparation

Standards were prepared in 0.02 M $NaClO_4$ with thorium concentrations varying from 20 ppt (86 pmol/L) to 600 ppt (2.6 nmol/L). An initial calibration curve was created using the standards prior to running any samples. In addition, one standard was introduced every 3 or 4 samples in order to check and correct for any potential fluctuations.

3.5 BET Surface Area Analysis

Surface area measurements were taken of the thorium oxide powders after immersion in the flasks at various pH levels in order to look at how the surface of the powder was affected. Surface area was analyzed using a Quantachrome Nova 1000 instrument using grade 5.0 nitrogen gas.

3.5.1 BET Method

Experimental surface areas are most commonly obtained through the analysis of adsorption isotherms of nitrogen or some other gas. In the case of explicit-model analyses such as the Brunauer-Emmett-Teller (BET) method the experimental isotherm is fit to a theoretically-obtained adsorption model, from which is extracted a monolayer capacity of the material. This capacity is a well-defined quantity and can be used compare experimental and simulated systems. In order to convert to a surface area, a value for the monolayer density is needed, which is obtained experimentally using a reference system of known surface area. The accuracy of this method requires that the monolayer density be transferable; that it is not dependent on the surface curvature or pore structure, and not strongly dependent on the chemistry of the underlying surface. The Nova 1000 surface area is shown in Figure 3.5.

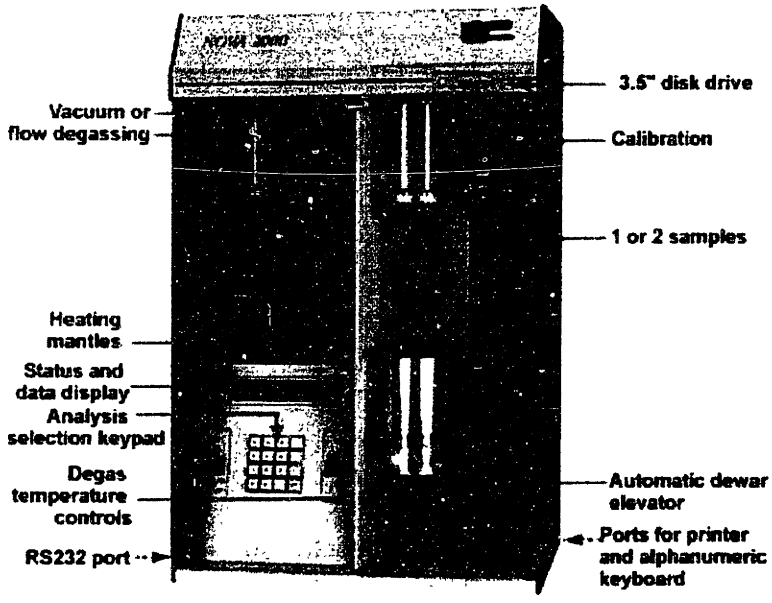

Figure 3.5 Quantachrome Nova 1000 BET surface area analyzer [32]

The tendency of all solid surfaces to attract surrounding gas molecules gives rise to a process called gas sorption. Monitoring the gas sorption process provides a wealth of useful

information about the characteristics of solids. Before performing gas sorption experiments, solid surfaces must be freed from contaminants such as water and oils. Surface cleaning (degassing) is most often carried out by placing a sample of the solid in a glass cell and heating it under a vacuum. Once clean, the sample is brought to a constant temperature by means of an external bath. Then, small amounts of a gas (the absorbate) are admitted in steps into the evacuated sample chamber. Absorbate molecules quickly find their way to the surface of every pore in the solid (the adsorbent). These molecules can either bounce off or stick to the surface. Gas molecules that stick to the surface are said to be adsorbed. Figure 3.6 shows this process. The strength with which adsorbed molecules interact with the surface determines if the adsorption process is to be considered physical (weak) or chemical (strong) in nature.

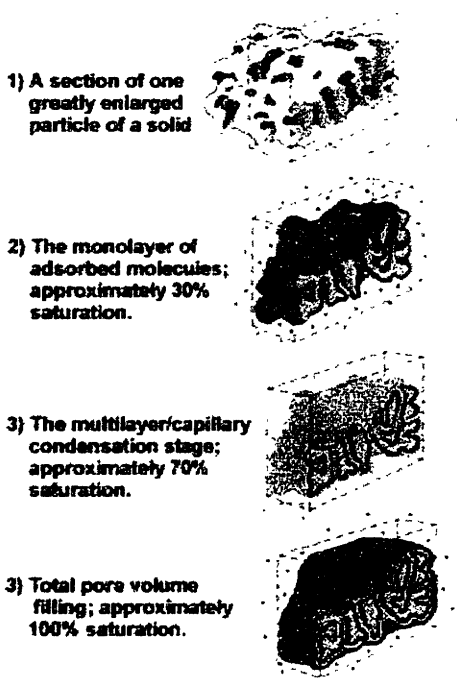

Figure 3.6 Surface adsorption of a gas

3.5.2 Sample Preparation

The thorium oxide remaining in the flask at the end of each experiment was removed and placed in a 50 mL polypropylene centrifuge tube. Each sample was centrifuged for two to five minutes, and any excess liquid was removed with a plastic bulb pipette. The samples were then placed in a freeze drier overnight until completely dry.

3.5.3 Procedure

For each measurement, approximately 0.1 g of thorium oxide powder was placed into a preweighed sample tube. The sample was placed in a heating mantle and degassed at 300 °C for a minimum of three hours. After degassing, the sample and tube were removed and weighed in order to determine the degassed sample weight. The sample was then placed in a dewar of liquid nitrogen for analysis. Each sample was analyzed using a six point BET method a minimum of three times.

3.6 X-Ray Diffraction

X-ray diffraction (XRD) was used to look at the thorium oxide remnants after immersion in the various pH solutions and determine if any major changes of lattice parameter could be found. Both lattice parameter changes and surface area changes can affect the kinetics of thorium oxide dissolution.

3.6.1 Principles of XRD

X-ray diffraction is a versatile, nondestructive technique for quantitative analysis and qualitative identification of the various crystalline phases found in solid minerals and powders

[33]. Identification is achieved by matching the pattern with a known pattern in a crystallography database. Databases can contain over 70,000 phases [34]. XRD is based on Bragg's law:

$$n\lambda = 2d \sin\theta$$

Crystalline structures are composed of three-dimensional rectangular lattices arranged so that they form a series of parallel planes separated from each other by a distance d. The distance varies according to the characteristics of the material. In a crystal, the planes exist in a number of different orientations, each with its own d-spacing. To create a diffraction pattern, monochromatic x-ray beam of wavelength λ is projected into a crystalline material. As the beam moves over the sample, the angle of incidence θ changes. Diffraction occurs only when the distance traveled by the x-rays differs by a complete number *n* of wavelengths. This occurs when Bragg's law criteria are met. This is shown in Figure 3.7. A plot of the angular positions and intensities of the resulting peaks is compared to the database to determine the structure and composition of a crystalline material.

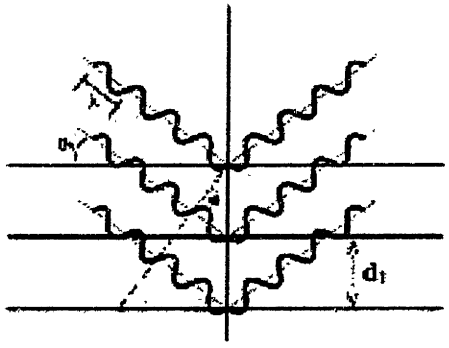

Figure 3.7 Bragg's Law

3.6.2 Sample Preparation

Samples of the dried thorium oxide remnants from the flask solutions were used for XRD. X-ray diffraction slides were prepared by combining approximately 100 mg of thorium oxide powder with 20 to 50 mg of standard material. Silicon carbide was used for the initial slides from the argon atmosphere experiments, and NIST traceable silicon 640c standards were used for the remaining samples. Standard materials were added in order to adjust for any shift in lattice parameter. The thorium powder/standard mixture was added to a three to one mixture of amyl acetate and collodium, stirred, and painted on a small piece of glass microscope slide cut to fit into the sample holder.

3.6.3 Procedure

Sample analysis was performed on a Rigaku RU300 x-ray generator with a 185 mm diffractometer operating at 60 kV and 300 mA (18 kW). Scans were performed for theta ranging from 20 to 80 degrees in steps of 0.05 degrees. 1.0 mm divergence and scatter slits were used, and a 0.3 mm receiving slit was used. Scans were analyzed for diffraction pattern matches using Jade.

3.7 Neutron Activation Analysis

Neutron activation analysis (NAA) was used to analyze carbonate samples with concentrations below the detection limits of ICP-AES. ICP-MS was not pursued any farther due to the remote proximity of the machine and difficulties with the high sodium

concentrations of the samples. Neutron activation was performed at the MIT Nuclear Reactor Laboratory's 5 MW research reactor.

3.7.1 Principles of Neutron Activation Analysis

Neutron activation analysis is a very sensitive detection technique. Like ICP-MS, it detects isotope, not just the element as in ICP-AES. In NAA, a sample is placed in a neutron flux, which is usually from a nuclear reactor, though accelerator driven sources now exist. The isotope absorbs neutrons, creating a new isotope. When this isotope decays it emits a characteristic gamma ray that can be used to detect the presence of the isotope. Concentrations can be determined directly from NAA if the reactor flux, time in flux, and detector efficiency are known. As this is usually not the case, samples are typically compared to a calibrated standard to determine concentrations of nuclides present.

For this experiment, samples were irradiated for 12 hours in the pneumatic facilities of the MIT reactor. Neutron flux in these facilities is approximately 8×10^{12} n/cm^{2}s. Samples were allowed to decay for approximately two weeks in order to get reduce the Na^{24} content to nearly zero.

3.7.2 Sample Preparation

Standard procedures at the MIT Nuclear Reactor allow liquid samples only under special circumstances. Because of this, samples had to be dried before irradiation. Initially, 1.5 mL was pipetted from each sample vial into a labeled bag, and the samples were freeze-

dried. Early NAA data showed the freeze-drying method to be inadequate, possibly because the vacuum was strong enough to pull out some of the solid salt left behind in the bag.

Samples were prepared for NAA by pipetting 0.5 mL into labeled bags. Each labeled bag was placed in a 50 mL centrifuge tube. The centrifuge tubes were placed in a large desiccator containing silica gel desiccant. The large desiccator could handle 36 samples at once. Once the desiccator was full, it was placed in an oven at 80 °C overnight to allow samples to dry. Dried samples were removed and then heat-sealed and double bagged.

3.7.3 Standard Preparation

NIST traceable fly ash standards were prepared and irradiated with each sample batch. In addition, 0.1 M $NaClO_4$ ICP standards were dried along with the samples in order to determine drying efficiency. Two ICP standards were prepared for each sample batch to ensure that any irregularities were not sample specific, but system wide. The ICP standards were prepared in the same manner as the regular samples. 0.5 mL was pipetted into a labeled bag, then placed in a desiccator overnight at 80 °C.

3.7.4 Procedure

Twelve to fourteen samples from the same flask were placed in each irradiation batch along with two ICP standards and a NIST fly ash standard. This was done to minimize the effects of any flux irregularities on the final data, as the entire data set would have experienced the same irradiation. All batches were irradiated for twelve hours. After a two-week decay, samples were counted on four Canberra high purity germanium detectors. The

fly ash standard from each irradiation batch was placed on each detector used for that batch for calibration. The Pa^{233} 312 keV gamma peak was used for all measurements. Samples were counted for six hours live time. A six-hour background was taken on each detector before sample counting began. In addition, an empty bag was irradiated in order to determine if there would be any background attributable to the bag. There was no noticeable background from either the bag or the room.

3.8 Fourier Transform Infrared Spectroscopy

Fourier transform infrared spectroscopy (FTIR) was used on the ThO_2 remnants to determine if anything had sorbed to or precipitated on the surface of the powder.

3.8.1 Principles of FTIR

Infrared spectroscopy is an experimental method employed to to study vibrational transition energies. Since atoms are not held rigidly apart in a molecule, they can bend or stretch. Each mode of vibration or stretching has one band of infrared absorption. When subjected to infrared radiation of that specific frequency, a bond will absorb the energy and move from the lowest to the next highest vibrational state [35]. Figure 3.8 shows the basic setup of an FTIR spectrometer.

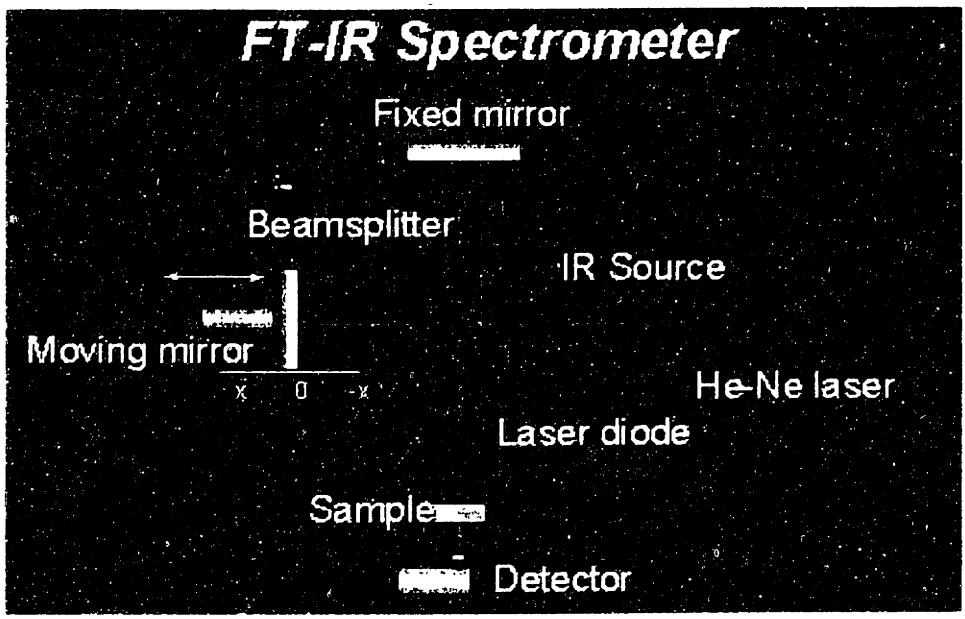

Figure 3.8 FTIR setup

3.8.2 Sample Preparation

FTIR samples were prepared by mixing about 20 mg of ThO_2 powder remnants with up to 200 mg KBr powder and grinding with a small agate mortar and pestle. The powder mixture was placed in a 13 mm die and pressed at 10 metric tons for three minutes. Ten samples were prepared, including a standard and an array of samples from each atmosphere. Table 3.2 lists the samples that were analyzed.

pH	Atmosphere
2.07	Ar
3.68	Ar
6.4	Ar
8.96	Ar
11.55	Ar
2.06	10% CO_2
3.6	10% CO_2
5.05	10% CO_2
6.48	10% CO_2

Table 3.2 FTIR Samples

3.8.3 Procedure

A Perkin Elmer 1600 series FTIR was used for sample analysis. One four second background was taken. Samples were scanned four times for four seconds each over the wavenumber range of 600 to 4000 cm^{-1}, and the background was removed from the spectra.

Chapter 4: Results

4.1 Solubility results

Several different methods were used to determine the aqueous thorium concentrations in the samples. ICP-AES was used for only the highest concentration samples. Samples below the detection limits of the ICP-AES method were analyzed using either ICP-MS or neutron activation analysis.

4.1.1 ICP-AES Data

The detection limit of the ICP-AES for the Th 401.913 nm line was approximately 0.2 μmol/L. Because of this limit, only samples from pH 2 through 3 under argon and ph 2 and 2.5 under 10% CO_2 could be analyzed using this method. A Cetac 6000AT$^+$ ultrasonic nebulizer was used in order to attempt to detect lower concentrations. While the detection limit for thorium in 5 vol% nitric decreased by a factor of twelve, the ultrasonic nebulizer proved to be ineffectual for the sample matrix due to the high content of sodium. The orange sodium flame was so bright that it completely interfered with the optics at all wavelengths.

Figure 4.1 is an example of a calibration curve from an ICP-AES analysis. This curve was used to fit the data for flasks 22 and 23, pH 2.06 and 2.57 under 10% CO_2.

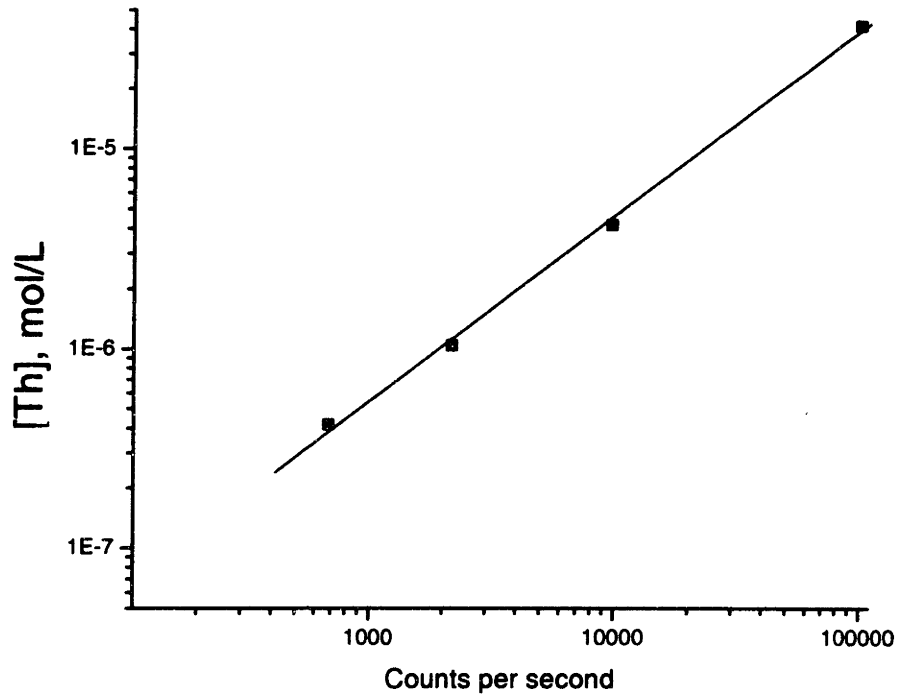

Figure 4.1 Standard calibration curve example

Figures 4.2 through 4.4 are the curve fits for kinetics data from the argon experiments at pH = 2.07, 2.57, and 3.00 respectively. All points on these curves were obtained using ICP-AES. Calibration curves for this data are in Appendix A. Curves were fit in Origin, using the equation

$$[\mathrm{Th}] = [\mathrm{Th}]_{sat}(1 - e^{-kt})$$

where $[\mathrm{Th}]_{sat}$ is the equilibrium concentration in mol/L, and k is the kinetic rate constant in hr^{-1}.

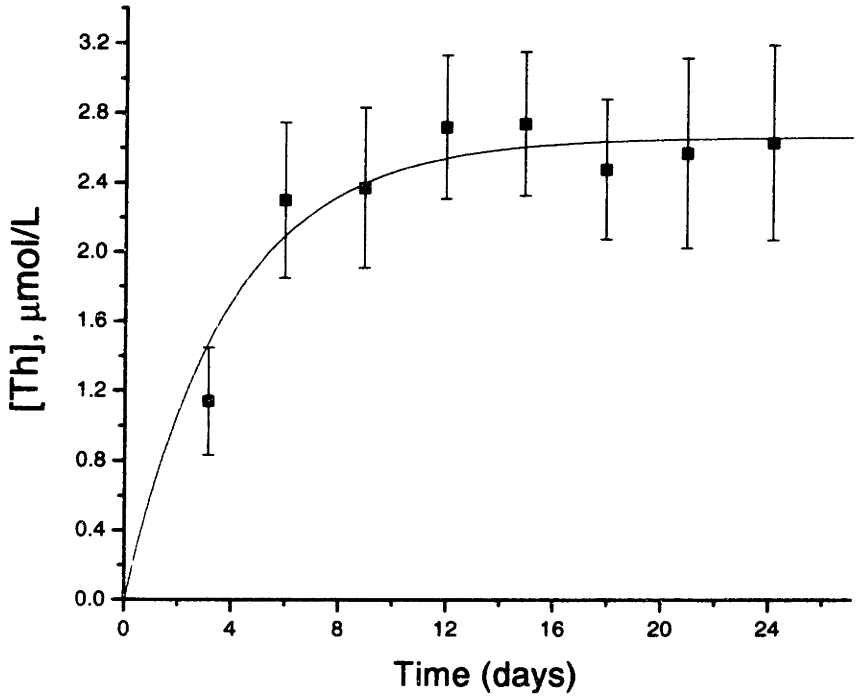

Figure 4.2 Kinetics curve for pH = 2.07, Argon

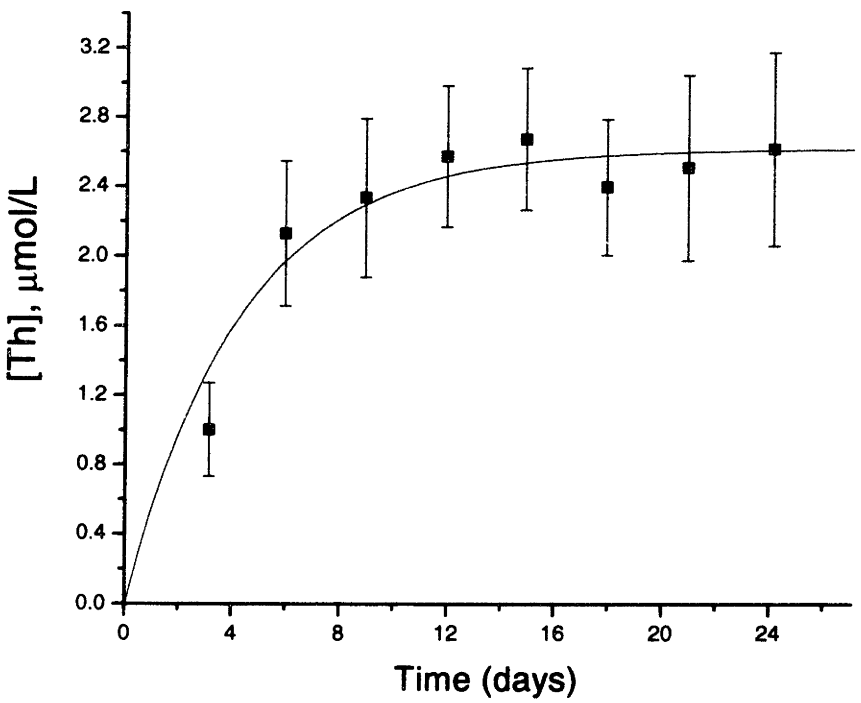

Figure 4.3 Kinetics curve for pH = 2.57, Argon

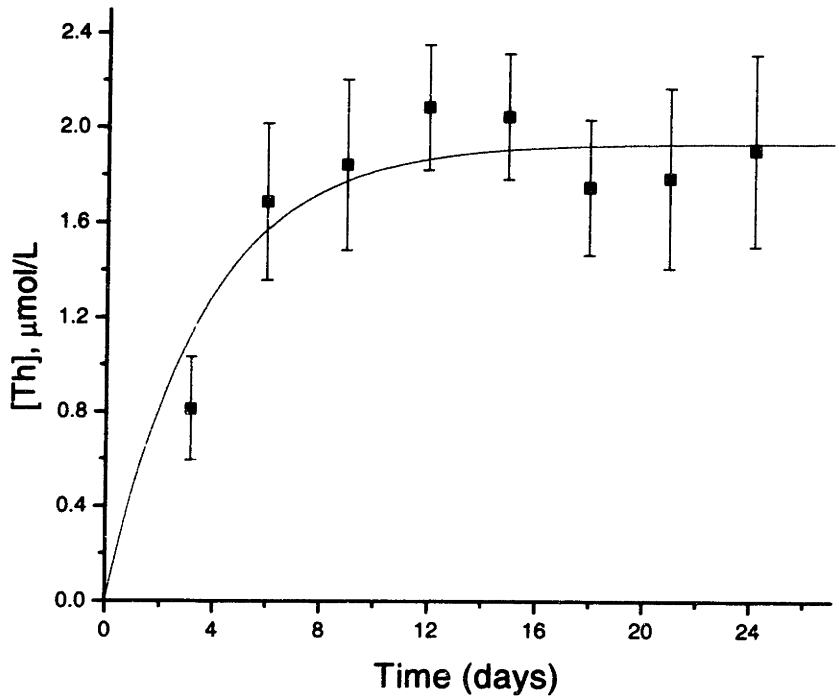

Figure 4.4 Kinetics curve for pH = 3.0, Argon

The initial ICP-AES data set for pH 2.06 and 2.57 from the carbonate series had to be thrown out due to excessive fouling of the torch from several high sodium concentration experiments that were run over a relatively short period of time. Enough volume remained for ICP-AES analysis of only the latter half of the series, due to the fact that NAA samples had been prepared from the first six samples of each series. NAA data from the first two samples from each series was added to the ICP curve to fill in the holes. This data predates the problems with excessive vacuum on the freeze drier, as the samples were prepared for NAA when the vacuum pump was not operating properly and therefore evaporated under close to atmospheric pressure. Figures 4.5 and 4.6 show the curve fits for pH 2.06 and 2.57 under 10% CO_2.

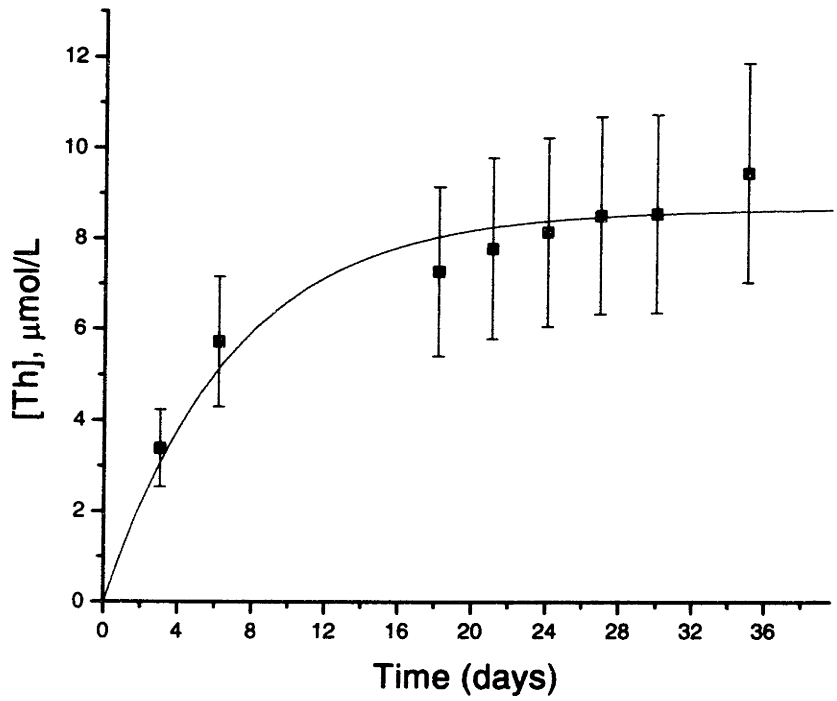

Figure 4.5 Kinetics curve for pH = 2.06, 10% CO_2

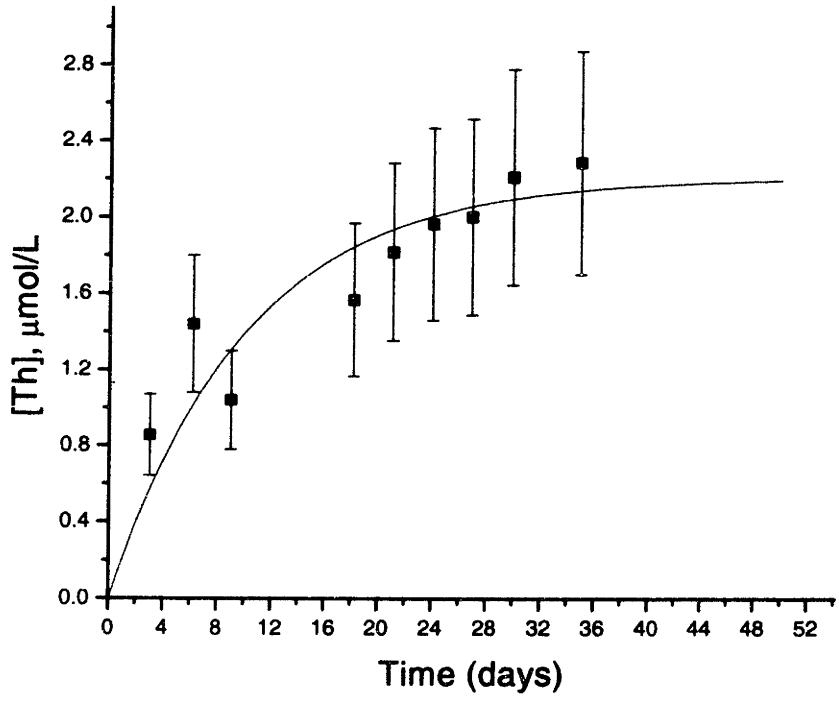

Figure 4.6 Kinetics curve for pH = 2.57, 10% CO_2

4.1.2 ICP-MS Data

The remainder of the argon sample series was analyzed using a quadropole inductively coupled plasma mass spectrometer with multicollection. Data gathering on this system proved to be difficult due to the high sodium content. Samples were diluted by a factor of five to minimize system instabilities. With this dilution factor and the system instabilities, however, many samples appeared to be below the detection limit of the instrument. No kinetics curves could be created from the data with any degree of certainty. The data is therefore only good for estimating equilibrium concentrations. Figure 4.7 shows the data and corresponding kinetics curve-fit for pH 6.9. The curve fit is meaningless due to the fact that only two of the 14 samples in the series could be successfully analyzed.

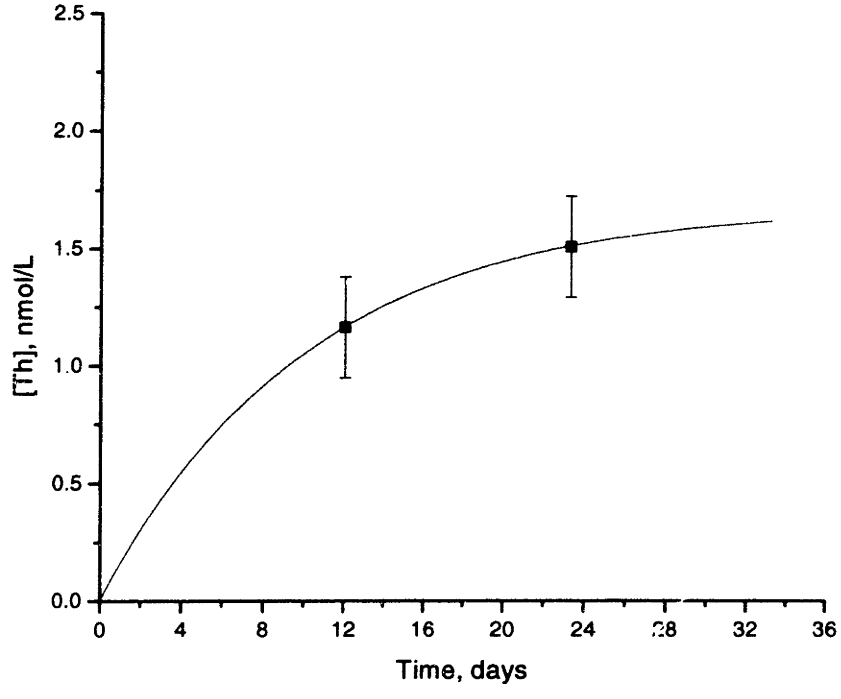

Figure 4.7 Kinetics curve for pH = 6.9, argon

The figures for the rest of the flasks are in Appendix A. Table 4.1 shows the saturation concentrations at each pH analyzed. Saturation concentrations were estimated as the average of all the data points for each experiment. Standard deviations were calculated from all of the data points as well. Several pH steps are missing because all of the data was either erratic or below the detection limit of the instrument.

pH	$[Th]_{sat}$, nmol/L
4.27	2.03 ± 0.48
6.40	3.26 ± 0.20
6.90	1.16 ± 0.35
7.38	2.84 ± 0.18
10.07	2.13 ± 0.46
12.04	2.46 ± 1.56

Table 4.1 $[Th]_{sat}$ vs. pH under 100% Argon

4.1.3 Neutron Activation Analysis Data

All carbonate samples below the detection limit of the ICP-AES were analyzed using neutron activation analysis. Samples were irradiated for 12 hours and allowed to decay for two weeks. Samples were counted on HPGe detectors for six hours and concentrations were determined by comparison to a NIST SRM Fly Ash 1633b standard. Table 4.2 shows the composition of the fly ash standard. The data was corrected for sample matrix effects using two matrix standards that were prepared and irradiated with each sample set. Matrix standard concentrations were 0.418 and 0.0418 μmol/L.

Element name	Elemental conc. (µg/g)	Error (µg/g)
Na^{23}	2010	30
Sc^{45}	41	1.5
Cr^{50}	198.2	4.7
Fe^{56}	77800	2300
Co^{59}	50	1.2
Se^{74}	10.26	0.17
As^{75}	136.2	2.6
Br^{81}	2.9	0.4
Ba^{130}	7.9	27
La^{139}	94	2.8
Ce^{140}	190	4.7
Nd^{146}	84	4.7
Eu^{151}	4.1	0.15
Sm^{152}	20	0.9
Lu^{175}	1.2	0.15
Hf^{180}	6.8	0.24
Ta^{181}	1.8	0.05
Th^{232}	25.7	1.3
U^{238}	8.79	0.36

Table 4.2 Fly Ash composition

Figures 4.8 through 4.15 show the neutron activation analysis data. This data was validated by running a second experiment at pH = 3.00. The data from the repeated experiment is shown in Figure 4.16. for pH 3 through 5.05, the equilibrium concentration was taken as the average of all of the data points. Experiments with pH greater than 5.05 all showed a peak in concentration between day six and day nine, then returned to the initial concentration. Since the peaks are close to or within the margin off error, it is possible that they are a coincidence. These experiments will be repeated in order to see if this is the case.

No kinetics data could be determined from the samples analyzed by NAA. It is also not possible to prove that the samples achieved equilibrium due to the lack of kinetics data. The acidic samples (pH 2 and 2.5) indicated that equilibration times were on the order of two months, twice as long as these experiments were run.

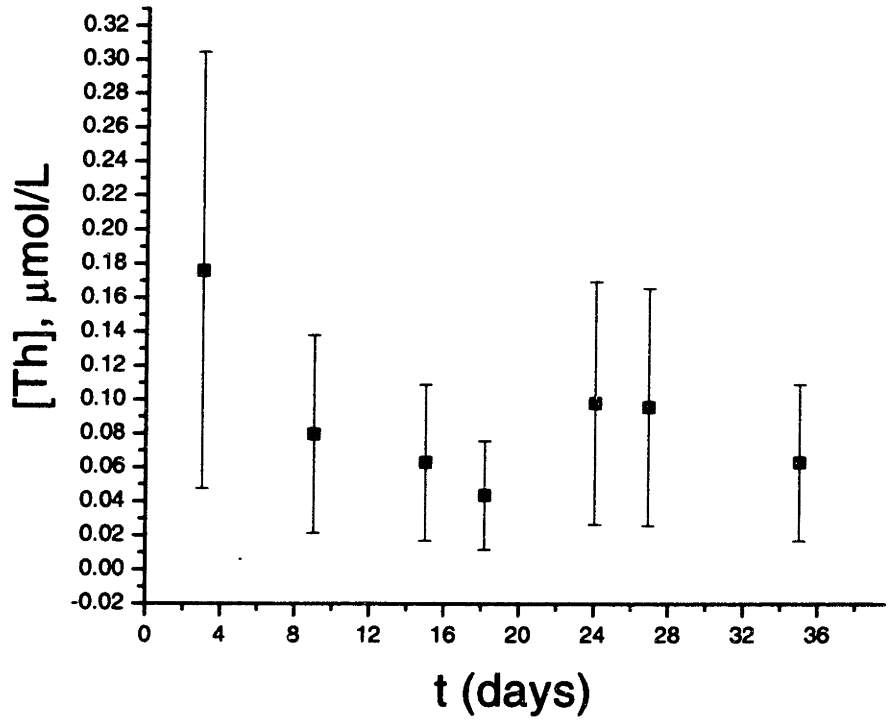

Figure 4.8 Data for pH = 3.10, 10% CO_2

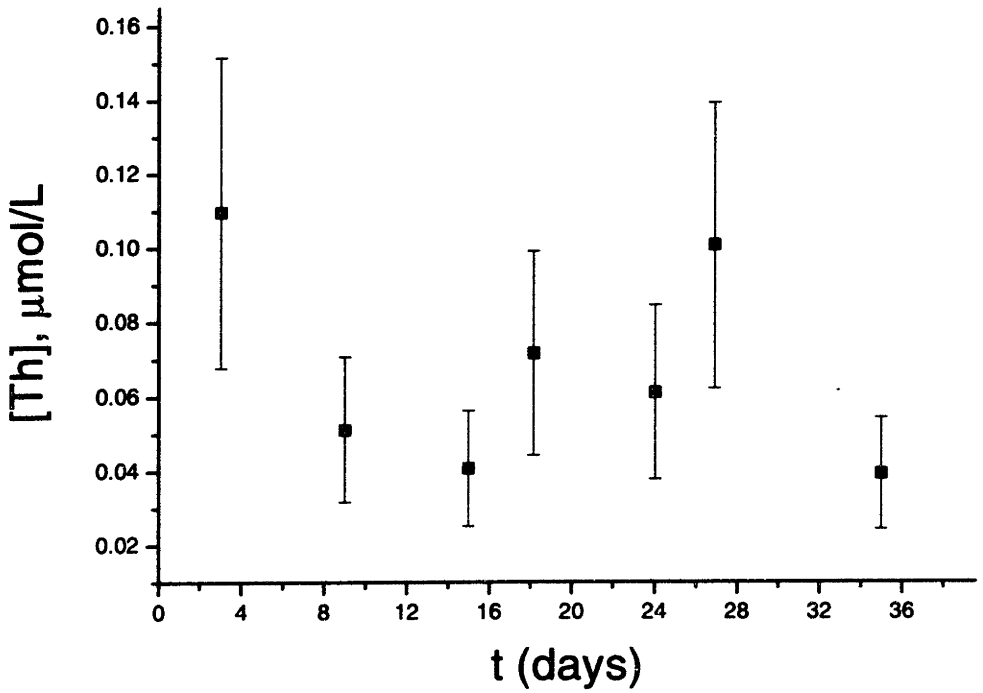

Figure 4.9 Data for pH = 3.60, 10% CO_2

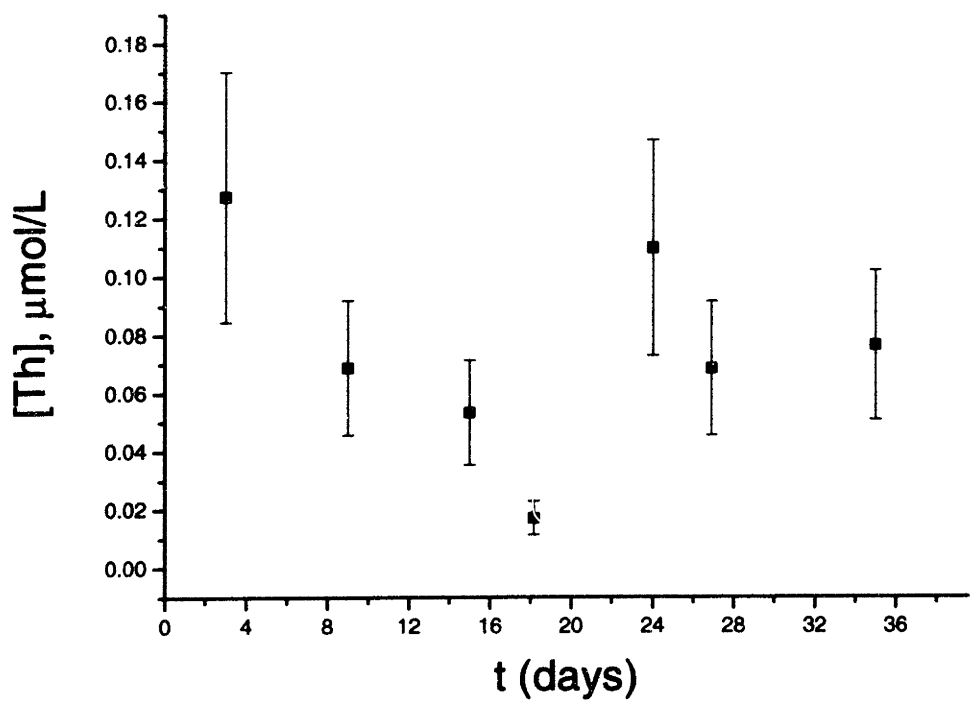

Figure 4.10 Data for pH = 4.13, 10% CO_2

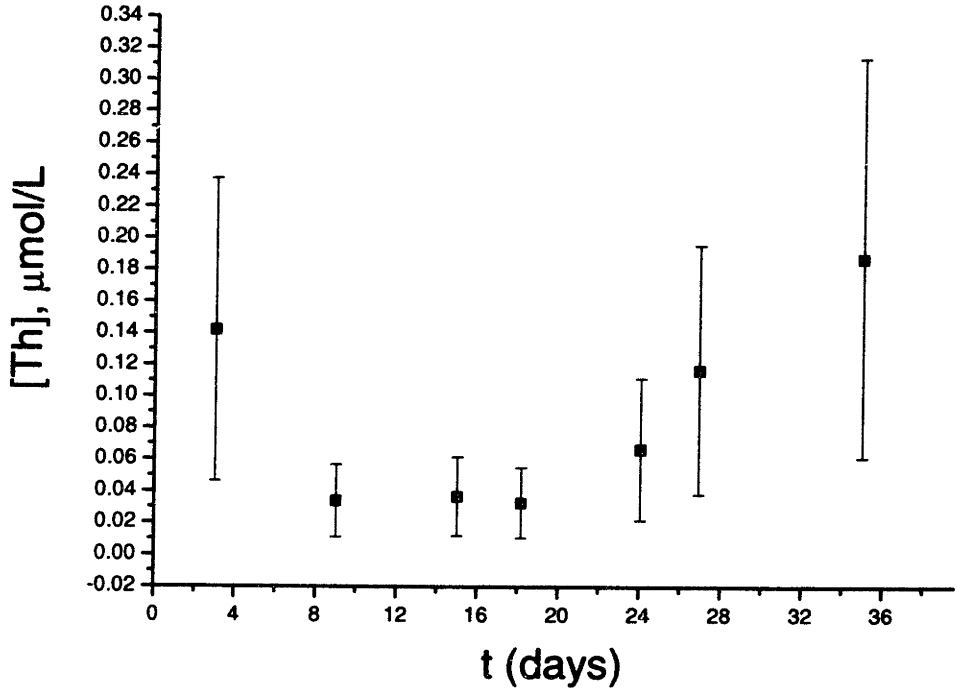

Figure 4.11 Data for pH = 4.48, 10% CO_2

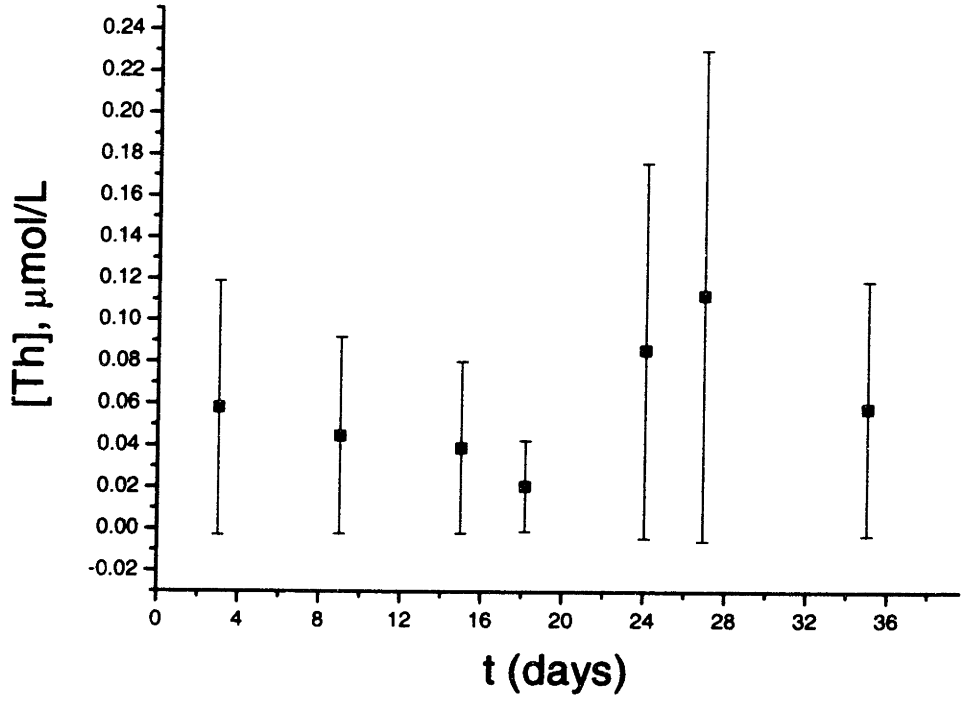

Figure 4.12 Data for pH = 5.05, 10% CO_2

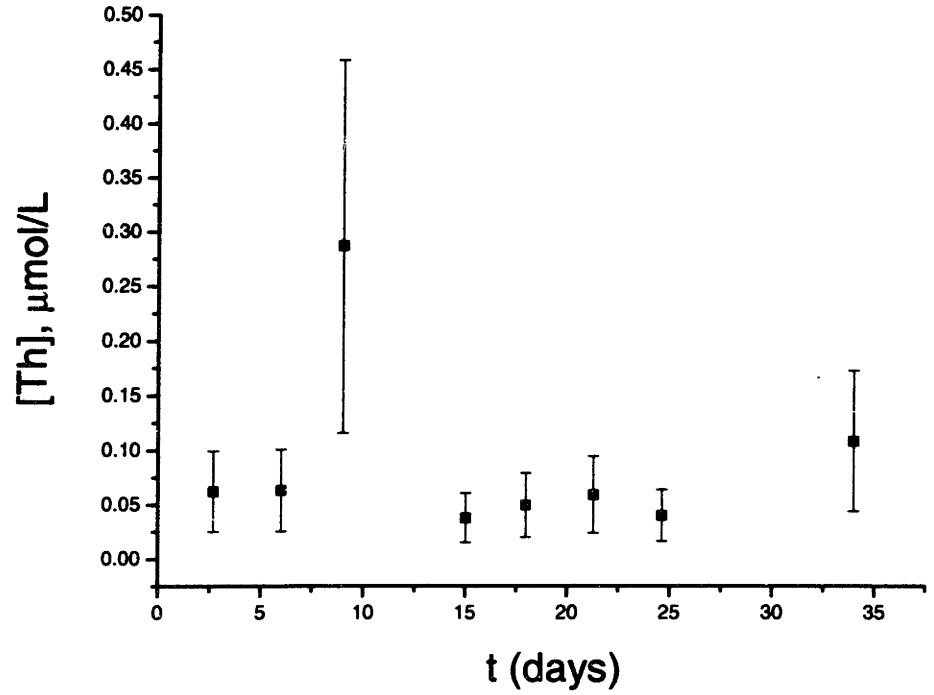

Figure 4.13 Data for pH = 5.51, 10% CO_2

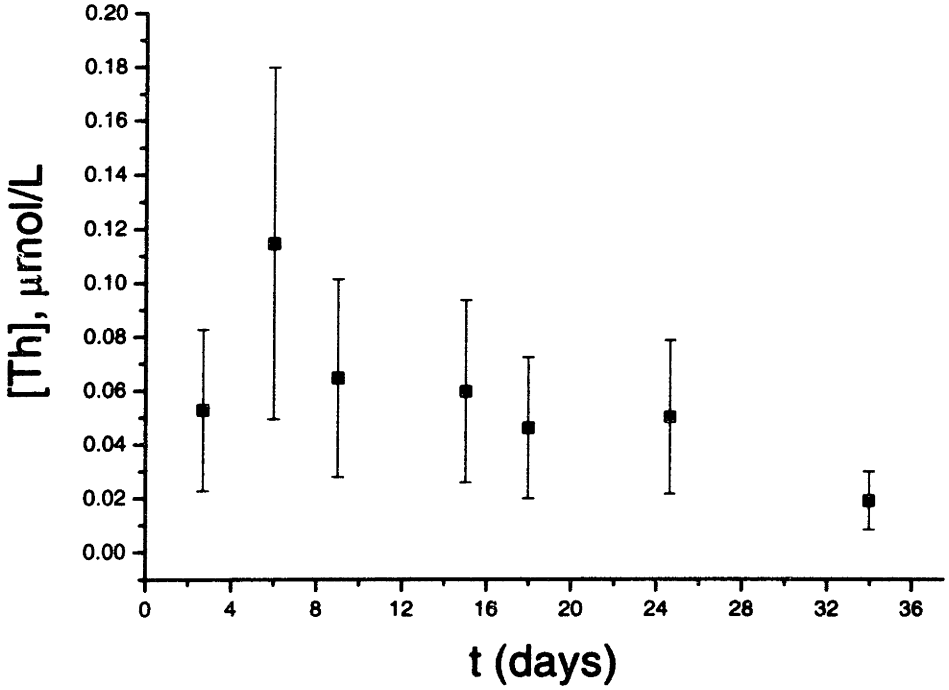

Figure 4.14 Data for pH = 6.03, 10% CO_2

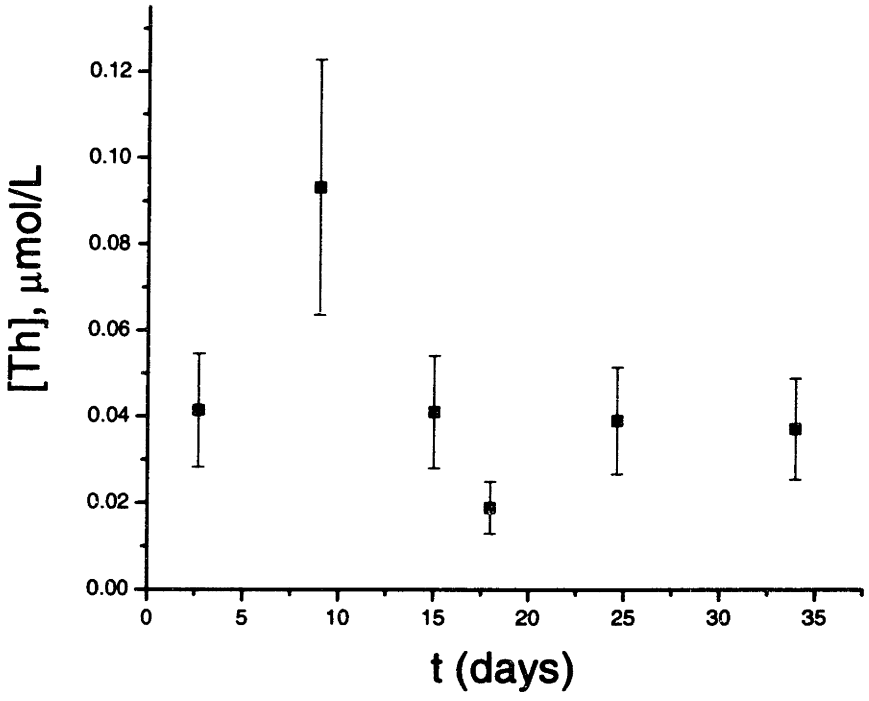

Figure 4.15 Data for pH = 6.48, 10% CO_2

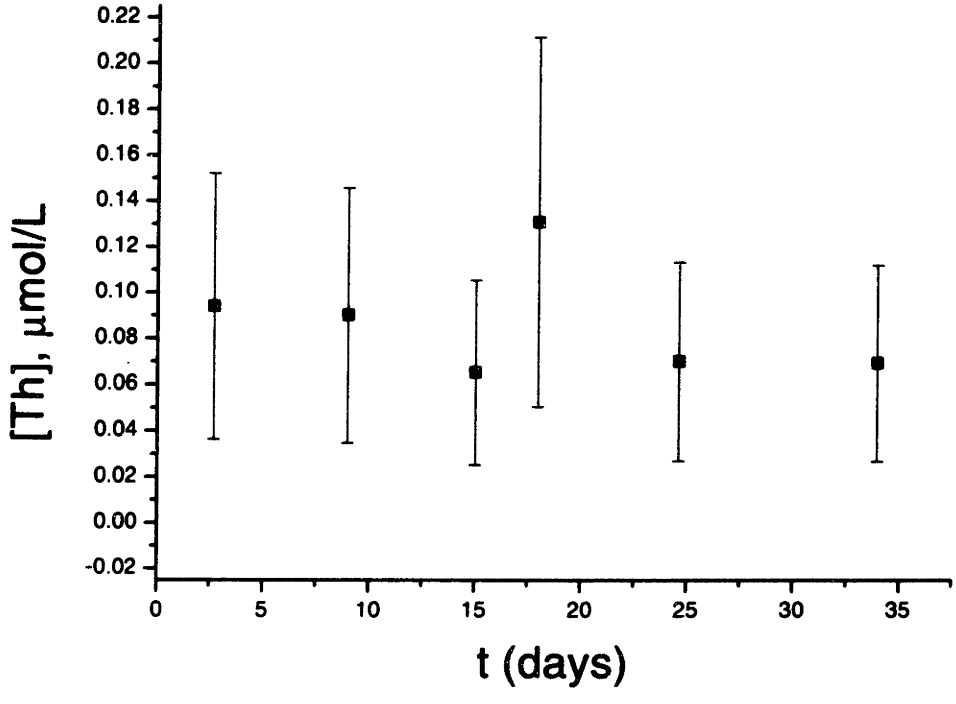

Figure 4.16 Data from pH = 3.00, 10% CO_2, experiment repeated

4.1.4 Large Colloids

Unfiltered samples were taken every nine days in conjunction with the filtered samples in order to determine if any large colloids (greater than 0.20 μm) were forming in the solutions. Analysis of these samples showed in general no significant change between the filtered and unfiltered samples. Bundschuh *et al* reported colloid sizes of about 20 nm [34], which is an order of magnitude lower than the filter size of 0.20 μm, so it is likely that any colloids formed were in the filtered samples as well. Filtered and unfiltered concentrations can be found in Appendix B.

4.1.5 Kinetics and Saturation

Using the data from these three methods, a plot of $[Th]_{sat}$ vs. pH can be created. Figure 4.17 shows the argon data, and the carbonate data is in Figure 4.18. When the carbonate system is recalculated for atmospheric CO_2 concentrations, or $pCO_2 = 10^{-3.5}$, the data is extended to pH = 11.38. Kinetics and saturation data is shown in Tables 4.3 and 4.4 for the argon and 10% CO_2 atmospheres, respectively.

Under the 100% argon cover gas, equilibrium was reached in a slightly less than one month in acidic solutions. The rate constants are all approximately equal, within the margins of error. No kinetics data could be extracted from the neutral and alkaline solutions. Under 10% CO_2, the equilibration time increased to two months for the most acidic samples. Once again, the other solutions did not yield any useful kinetics data. While it was assumed that

equilibrium was achieved, this cannot be proven. Experiments will have to be repeated in order to see if the equilibration time was sufficient.

From Figure 4.17, it can be seen that the solubility drops dramatically after pH 3, by a full three orders of magnitude in a step of 0.5 pH. This slope of –6 corresponds with drops reported in the literature. Rai et al showed a slope of -5.5 for amorphous ThO_2 [36], and a slope og greater than –4 was given in a literature review by Neck [37]. The carbonate system solubility decrease is less dramatic, with a slope of –3.3.

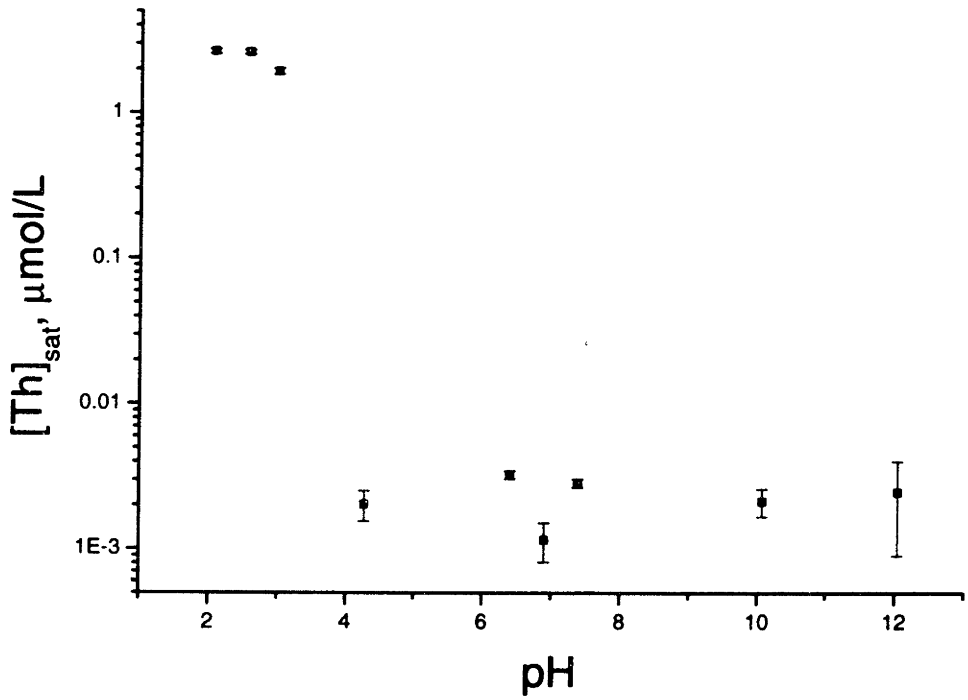

Figure 4.17 $[Th]_{sat}$ vs. pH, 100% Argon

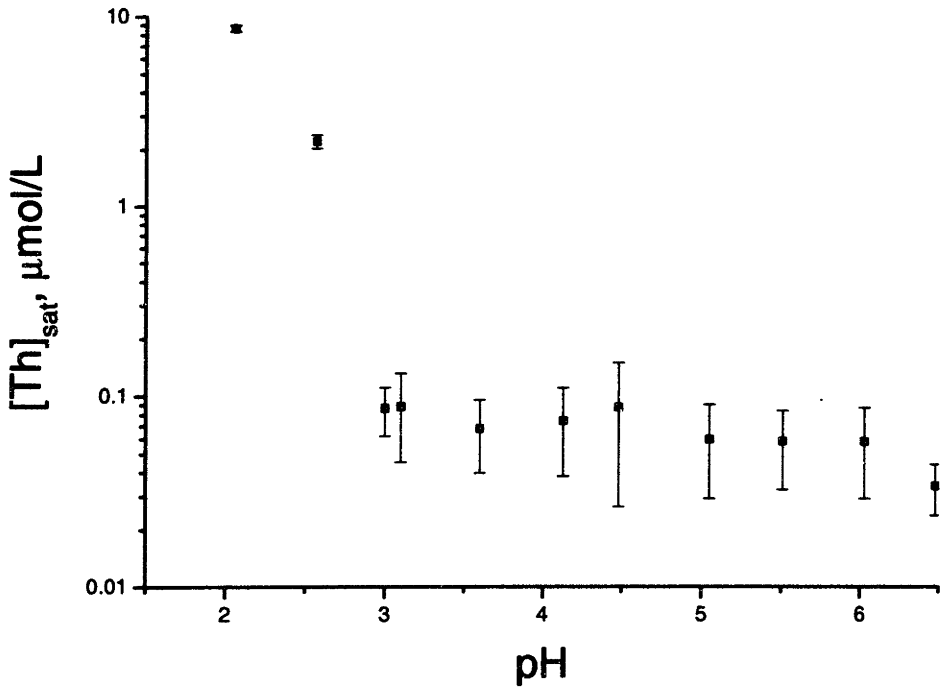

Figure 4.18 $[Th]_{sat}$ vs. pH, 10% CO_2

pH	k (h^{-1})	$[Th]_{sat}$, mol/L
2.07	0.01078 ± 0.00185	2.66E-06 ± 9.29E-08
2.57	0.00981 ± 0.00162	2.62E-06 ± 9.21E-08
2.99	0.01158 ± 0.00275	1.93E-06 ± 8.97E-08
4.27	-	2.03E-09 ± 0.48E-09
5.45	-	
6.40	-	3.26E-09 ± 0.20E-09
6.90	-	1.16E-09 ± 0.35E-09
7.38	-	2.84E-09 ± 0.18E-09
8.08	-	
8.60	-	
6.96	-	
9.52	-	
10.07	-	2.13E-09 ± 0.46E-09
10.60	-	
11.08	-	
11.55	-	
12.04	-	2.46E-09 ± 1.56E-09

Table 4.3 Kinetics and Saturation Data, 100% Argon

pH	k (h^{-1})	$[Th]_{sat}$, mol/L
2.06	0.00605 ± 0.00122	8.66E-06 ± 3.15E-07
2.57	0.00416 ± 0.00122	2.21E-06 ± 1.79E-07
3.00	-	8.67E-08 ± 2.47E-08
3.10	-	8.85E-08 ± 4.32E-08
3.60	-	6.78E-08 ± 2.80E-08
4.13	-	7.45E-08 ± 3.62E-08
4.48	-	8.79E-08 ± 6.14E-08
5.05	-	5.98E-08 ± 3.06E-08
5.51	-	3.40E-08 ± 1.02E-08
6.03	-	5.81E-08 ± 2.89E-08
6.48	-	3.40E-08 ± 1.02E-08

Table 4.4 Kinetics and Saturation Data, 10% CO_2

4.2 BET surface area analysis

A Quantachrome Nova 1000 BET surface area analyzer was used to determine the surface area of the thorium oxide remaining in the flask following each experiment. For each sample, a 6 point BET method was used. Samples were degassed at 300 °C for one to three hours prior to analysis. Comparison of sample weights and BET analysis results after degassing periods of one to twelve hours showed no significant advantage for degassing times longer than one hour.

Figure 4.19 shows the BET analysis results for the argon atmosphere samples. The red line corresponds to the measured value of an untreated thorium oxide sample from the same batch that was used for the experiments. The green dashed lines represent the upper and lower bounds of the untreated surface area. Figure 4.20 shows the BET analysis for the carbonate samples. The red and green lines represent the same untreated thorium oxide data as in the argon samples.

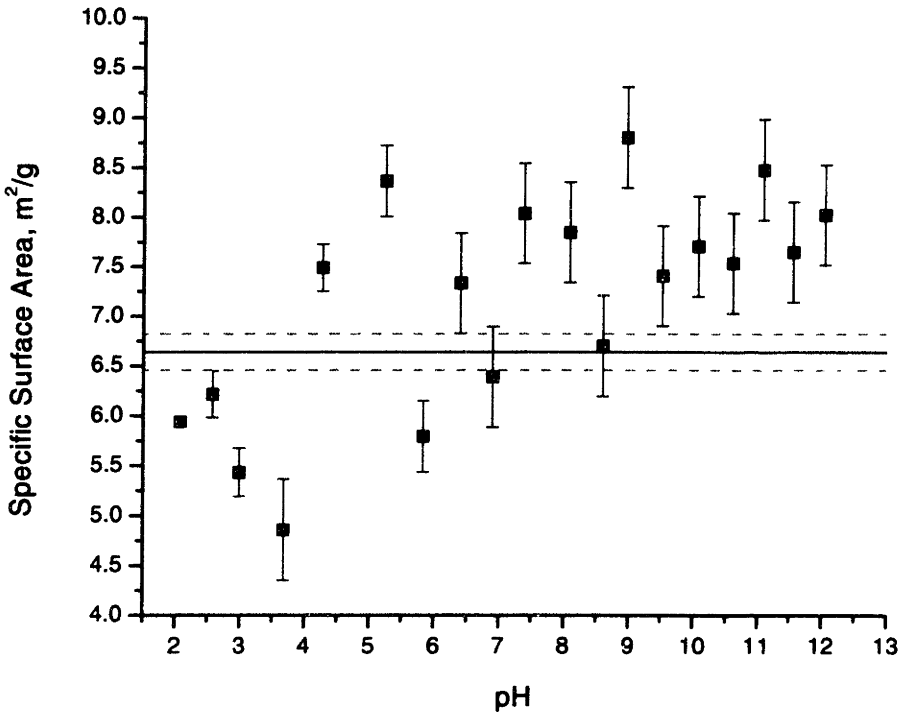

Figure 4.19 Surface area vs. pH, 100% Argon

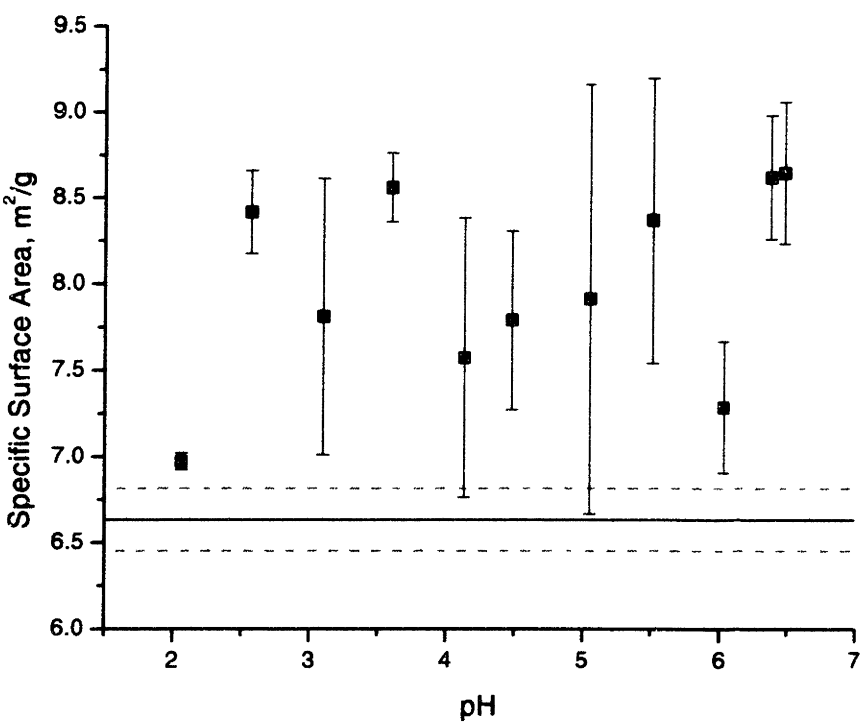

Figure 4.20 Surface area vs, pH, 10% CO_2

Under the 100% argon atmosphere, surface areas were widely scattered around the untreated sample standard until pH 9 and above, when the surface areas were uniformly higher than the standard by about 15%. Surface areas of the samples immersed in the carbonate systems were higher than the standard for all samples. The lowest pH sample, at around pH = 2.07, was very close to the upper bound of the untreated surface area. The remaining samples had surface areas 15 to 30% higher.

4.3 XRD Results

X-ray diffraction patterns were taken of the thorium oxide remnants from each experiment. The XRD scans were taken on a Rigaku RU300 x-ray generator with a 185 mm diffractometer. Scans were taken in steps of 0.05 at a speed of 10 degrees per minute. The scan range was from 20 to 80 degrees. Figure 4.21 shows the scan for the untreated ThO_2 standard. Each ThO_2 peak is labeled with the corresponding plane. Unlabeled peaks belong to the Si standard. A scan of the pH = 6.48 carbonate sample is shown in Figure 4.22. All of the samples immersed in the solutions had identical lattice parameters to the untreated sample. The d-spacings are listed in Table 4.6 below. The remaining XRD scans can be found in Appendix C.

(*h*,*k*,*l*)	d, Å
(1,1,1)	3.232
(2,0,0)	2.799
(2,2,0)	1.9987
(0,1,0)	1.6877
(2,2,2)	1.6159
(4,0,0)	1.3983
(3,3,1)	1.2841
(4,2,0)	1.2516

Table 4.6 Planes and d-Spacings of ThO_2

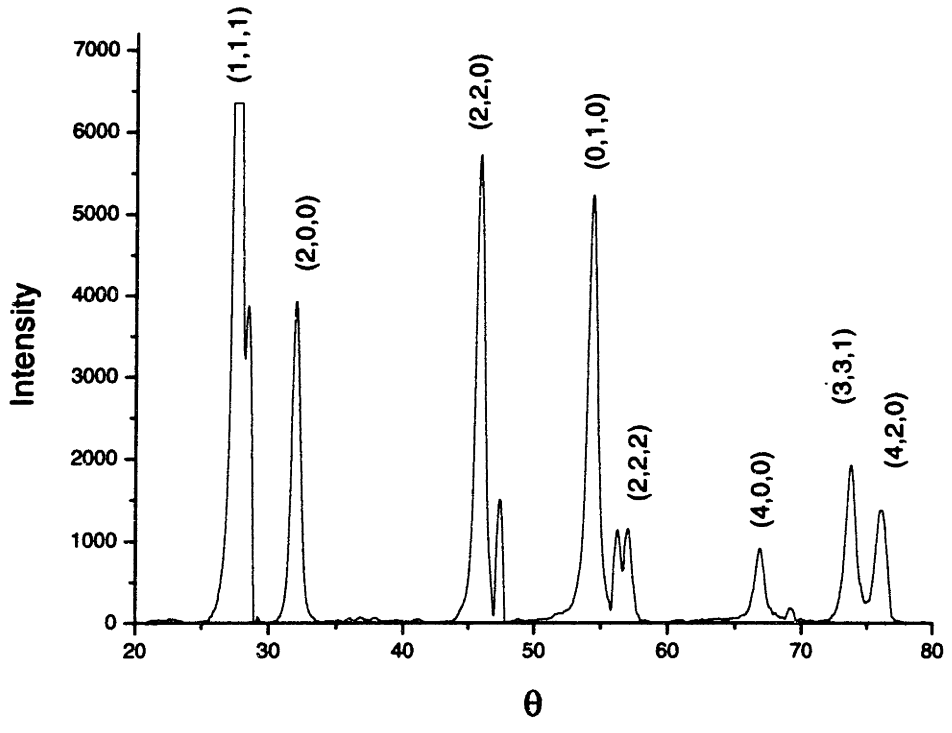

Figure 4.21 Untreated ThO_2 XRD Pattern

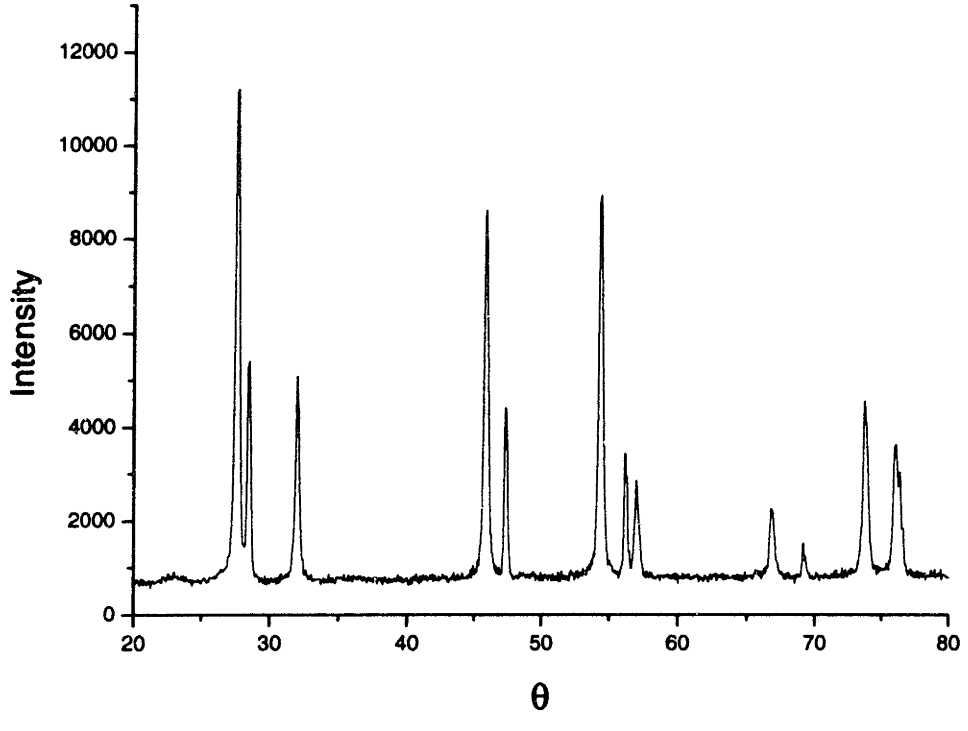

Figure 4.22 XRD pattern for pH = 6.48, 10% CO_2

4.4 FTIR Results

FTIR was used to determine if anything had sorbed to or precipitated on the surface of the ThO_2 remnants from the solution. A Perkin Elmer 1600 series FTIR was used. Four 4.0 second scans were taken of each pellet. Figure 4.23 shows the FTIR spectra of the untreated sample. The basic features of this spectra were repeated in the spectra of all samples scanned with the exception of pH 3.68, under 100% argon. This sample was a different color from the rest, dirty brown instead of white. The sample was most likely contaminated at some point while stored. All of the FTIR spectra are included in Appendix D. There is no spectra for the 100% argon, pH = 2.07 sample because the pellet broke while being placed in the sample holder.

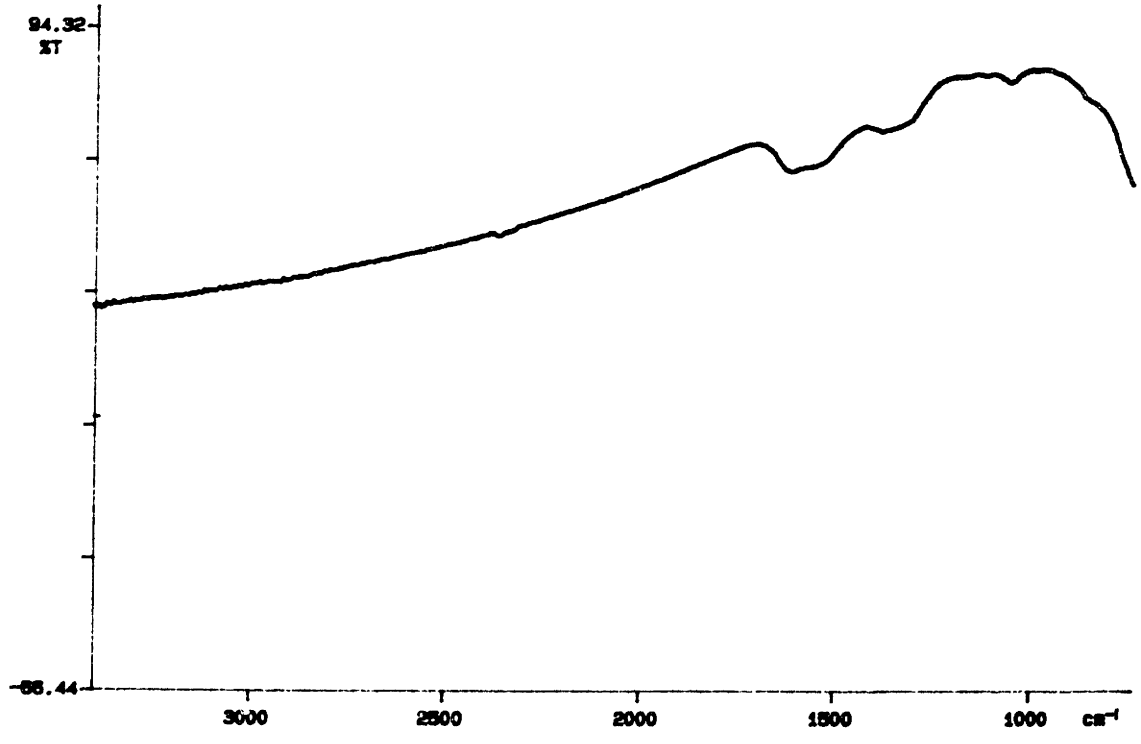

Figure 4.23 FTIR spectrum of ThO_2 standard

All of the major features of the sample spectra corresponded well with the ThO_2 spectrum from Nyquist and Kagel [37]. A standard spectrum from the Japanese National Institute of Advanced Industrial Science and Technology is shown in Figure 4.24 [38].

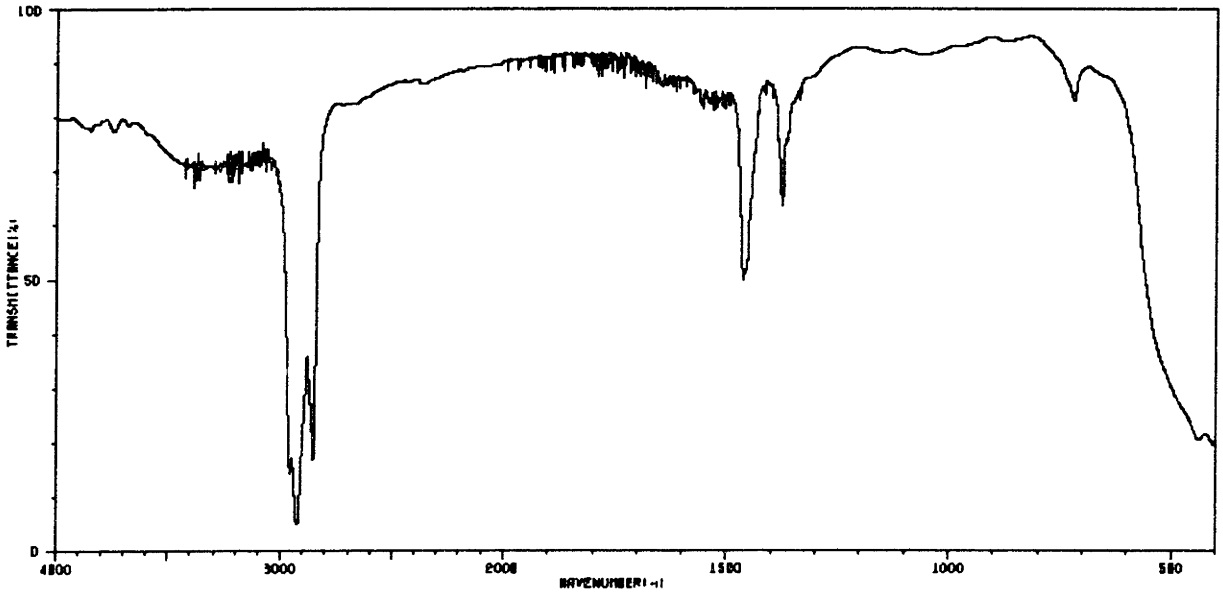

Figure 4.24 ThO_2 Standard spectrum

Chapter 5: Conclusion

Interest in thermal breeder reactors using a thorium-uranium fuel has increased recently as research into the next generation of nuclear power reactors has intensified. Since it is going to be a once through fuel cycle, it is important to study the behavior of the fuel in long term storage. The first step in understanding this behavior is to characterize the behavior of the fuel components in the environment. Uranium oxide has been well studied in its two major forms, UO_2 and U_3O_8 due to the prevalence of this fuel in nuclear fuel cycles worldwide. The behavior of thorium oxide is not as extensively studied as its uranium counterparts. In order to gain a better understanding of thorium oxide dissolution, a broad study of the kinetics and thermodynamics of thoria dissolution was undertaken.

The dissolution kinetics of crystalline thorium oxide were studied over a broad pH range and under both pure argon and a mixture of 90% argon and 10% CO_2 in 0.1 M ionic strength $NaClO_4$ solution. Under pure argon, the pH range was 2 through 12 in steps of 0.5. The CO_2 pH ranged from 2 to 6.5 in steps of 0.5. The maximum pH was limited to 6.5 due to buffering by the carbonic acid system. Experiments ran for 33 days, with sampling intervals of approximately three days. Every third time, an unfiltered sample was taken in conjunction with the filtered sample in order to determine if any colloids were forming. Remnants of the ThO_2 powder were removed from solution after each experiment for XRD, BET surface area analysis, and FTIR spectroscopy.

Results of the experiments showed that thorium oxide is a very stable and insoluble compound. Solubility is highest at very low pH, generally less than around 3. This is the pH region where the hydrolysis reaction is believed to be dominant, and $ThO_2(cr)$ and $Th^{4+}(aq)$

are in equilibrium [37]. Saturation concentrations varied from nanomolar under argon in neutral and alkaline conditions to 10 μmol/L under 10% CO_2 at pH of about 2. Solubility under CO_2 reached a minimum of about 50 nanomoles per liter, about an order of magnitude higher than the 100% argon counterparts. There was a very steep and rapid drop in concentration between the two solubility ranges. The slope was –6 for argon, and –3.3 for the carbonate system.

Kinetics data showed that the solutions reached equilibrium in under a month under the pure argon atmosphere at low pH, and in about two months under 10% CO_2 for pH 2.5 and below. It is possible that colloidal interactions or precipitation reactions could be slowing down the dissolution kinetics in the carbonate system at these pH levels. No kinetics data could be determined from the samples above pH 3 under argon and pH 2.57 under carbonate. Due to difficulties with system fluctuations from high sodium content, ICP-MS analysis of the argon neutral and alkaline samples yielded sporadic and scattered data. Most samples could not be analyzed by the instrument. Equilibrium concentrations were approximated as the average of the data yielded by the instrument. Samples above pH 2.57 in the carbonate system were analyzed by neutron activation analysis. Though the quality of this data was superior to the ICP-MS data, it also failed to yield any useful kinetics data. All samples appeared to be about the same concentration. Once again, the equilibrium concentration was approximated as the average of the sample concentrations. It is not certain that equilibrium was achieved in any of these experiments, due to the lack of reliable kinetics data.

Analysis of the thoria remnants from the experiments revealed that the harsh environments had little or no effect on the thoria powder in the flask. Initial surface area was approximately 6.7 m^2/g as measured by BET surface area analysis. Under pure argon, the

surface area increased by an average of about 15% under the most alkaline conditions. Below pH 10, the data was scattered around the untreated thoria standard. In the carbonate environment, all of the samples showed an increase over the initial untreated surface area. The increase was relatively uniform and ranged from 15 to 30%.

XRD analysis showed that all of the samples were identical to the untreated powder. All planes and plane spacings corresponded exactly with the standard. FTIR analysis also showed that there were no impurities or changes in composition or structure. Bundschuh *et al* concluded from their experiments that the bulk of the surface of their crystalline ThO_2 must have been covered in an amorphous layer of $Th(OH)_4$ under alkaline conditions [39], but there was no evidence of this structure in the FTIR spectra. It is possible that there was not enough present to show up in the spectra. In addition, no standard spectra of $Th(OH)_4$(am) could be found in the literature for comparison.

Studies at pH greater than about 2.5 will have to be repeated in the future in order to obtain kinetics data for comparison, as well as to determine if the previous experiments had reached equilibrium. Due to the detection limit problems encountered in these experiments with the various methods used, future experiments may employ Th^{228} doping in order to allow direct analysis of samples by an alpha/beta scintillation counter. In addition, the dissolution behavior of ThO_2 ceramics containing UO_2 and stabilized in a cubic fluorite ZrO_2 lattice will be studied in order to see both the effects of thoria and zirconia on urania dissolution. Preliminary modeling of the mixed thoria-urania solubility has been performed on CHESS and is included in Appendix E. Samples will be analyzed using the same methodology as the thoria dissolution experiments, including XRD, FTIR, and BET surface area analysis of ceramics before and after immersion. In the future, experiments on irradiated ceramics should

also be performed in order to investigate the effects of fission products in the lattice on the stability of the ceramic.

It is important to study all future nuclear reactor fuels from the perspective of long term waste behavior, especially given that indefinite storage in a repository is the nation's only plan for the disposition of spent nuclear fuel. These experiments have shown that crystalline thorium oxide would make a very robust waste form. Exposure to excessive pH for extended periods has little to no effect on the structure, and solubility is very low, especially in the pH range encountered in natural environmental systems.

References

1. Kazimi, Mujid et al. **Advanced Proliferation Resistant, Lower Cost, Uranium-Thorium Dioxide Fuels for Light Water Reactors,** Nuclear Energy Research Initiative Project 99-0153 Quarterly Report, May 2000

2. Eckhardt, Roger C.: Summary and Synthesis Report on Radionuclide Retardation for the Yucca Amount Site Characterization Project, Yucca Mountain Site Characterization Program Milestone 3784M, (October 1997).

3. Sherman, Christi. **Np(V) Sorption on Goethite, Montmorillonite, and Tuff**, Thesis, 2001

4. Gong, W.L.; Lutze, W.; Ewin, R.C. **Zirconia ceramics for excess weapons plutonium waste.** J. Nucl. Mat. (2000), 277, 239-249

5. Parrington et al, **Nuclides and Isotopes, fifteenth edition.** 1996 General Electric Co.

6. Crawford, C.L.; Biddle, C.R.; Bibler, N.E. **Durability testing of heavy-ion irradiated crystalline ceramics.** Report, WSRC-MS-2000-00309 http://www.srs.gov/general/sci-tech/fulltext/ms2000309/ms200309.html

7. De Lima, N.B. and Imakuma, K. **X-ray diffraction study of the formation of solid solutions in urania-thoria prepared by aqueous chemical processes.** J. Nuc. Mat. (1985), 135, 215-221

8. Benedict, Manson; Pigford, T.H..; Levi, H.W. **Nuclear Chemical Engineering 2nd Edition.** 1981 McGraw-Hill 318-321

9. Balek, Vladimir. **Application of emanation thermal analysis for characterization of intermediate products of urania and thoria ceramics.** J. Nuc. Mat. (1988), 153, 41-49

10. **Zirconium Dioxide**. Accutatus Ceramic Corporation, http://www.accuratus.com/Zirconium_Dioxide.htm

11. Curran, V.L. **Evaluation of Thorium Waste Behavior.** Report, MIT, August 2000 pp. 15-19

12. Oesthols, Eric. **The solubility of microcrystalline ThO_2 in phosphate media.** Radiochim. Acta (1995), 68(3), 185-90

13. Oesthols, Eric; Malmstrom, Maria. **Dissolution kinetics of ThO_2 in acid and carbonate media.** Radiochim. Acta (1995), 68(2), 113-119.

14. Akabori, Mitsuo; Sheratori, Tetsuo. **Dissolution of ThO_2-based oxides in nitric acid solutions at elevated temperatures.** J. Nucl. Sci. Technol. (1994), 31(6), 539-545
15. Felmy, A.R.; Rai, Dhanpat, Mason, M.J. **The solubility of hydrous thorium(IV) oxide in chloride media: development of an aqueous ion-interaction model.** Radiochim. Acta (1991), 55(4), 177-185

16. Ryan, Jack L.; Rai, Dhanpat. **Thorium(IV) hydrous oxide solubility.** Inorg. Chem. (1987), 26(24), 4140-2.

17. Zimmer, Erich; Merz, Eric. **Dissolution of thorium-uranium mixed oxides in concentrated nitric acid.** J. Nucl. Mater. (1984), 124 64-7

18. Takeuchi, Takeji; Hanson, C.K.; Wadsworth, M.E. **Kinetics and mechanism of the dissolution of thorium oxide in hydrofluoric acid and nitric acid mixtures.** J. Inorg. Nucl. Chem. (1971), 33(4), 1089-98

19. Sunder, S. and N.H. Miller. **XPS and XRD studies of $(Th,U)O_2$ fuel corrosion in water.** J. Nucl. Mat.(2000), 279(1), 118-126

20. Genthe, Ingmar; Lagemar, Bo. **Studies on metal carbonate equilibria – complex formation in the Th(IV)-H_2O-CO_2(g) system.** Acta Chem. Scand. 1991, 45, 231-238

21. Rai, Dhanpat et al. **Thermodynamic model for the solubility of thorium dioxide in the Na^+-Cl^--OH^--H_2O system at 23 °C and 90 °C.** Radiochim. Acta (2000), 88(5), 297-306

22. Heimann, R.B.; Vandergraaf, **Cubic zirconia as a candidate waste form for actinides – dissolution studies.** J. Mater. Sci. Lett. (1988), 7(6), 583-586

23. Momin, A.C.;Mirza E.B.; Mathews, M.D. **High temperature x-ray diffreactometric studies on the lattice thermal expansion behaviour of UO_2, ThO_2, and $(U_{0.2}Th_{0.8})O_2$ doped with fission product oxides.** J. Nucl. Mat. (1991), 185, 308-310

24. Takeuchi, T., Hanson, C.K., Wadsworth, M.E. *Journal of Inorganic Nuclear Chemistry*, 1971. 33 (1089-1098)

25. Shying, M.E., Florence, T.M., Carswell, D.J. **Oxide Dissolution Mechanisms II. Mechanism for the Thoria/Nitric/Hydrofluoric Acid System**, Journal of Inorganic Nuclear Chemistry, 1970. 32 (3493-3508)

26. Shying, M.E., Florence, T.M., Carswell, D.J. **Oxide Dissolution Mechanisms I. Role of fluoride in the thoria/nitric/hydrofluoric acid system.** Journal of Inorganic Nuclear Chemistry, 1972. 34 (213-220)

27. Palmer, D.A., van Eldyk, R. TITLE *Chemistry Revue*, 1983. 83, (651-731)

28. Östhols, E. and Malström, M. Dissolution Kinetics of ThO_2 in Acid and Carbonate Media, *Radiochimica Acta*, 1995. 68 (113-119)

29. Czerwinski, K. Nuclear Waste Management lecture notes, lecture 4.

30. Czerwinski, K. Waste Management Issues, MIT February 1999.

31. Gill, Robin, **Modern Analytical Geochemistry**, Longman Singapore Publishers, LTD, Singapore, Indonesia 1997 pp. 41-60

32. Quantachrome Incorporated, http://www.quantachrome.com/

33. Phillips Analytical, Introduction to X-ray Diffraction, http://www-us.analytical.phillips.com/technologies/xrd/

34. International Crystal Diffraction Database, http://www.icdd.com/

35. Ryan, J.L. and Rai, D. Thorium(IV) Hydrous Oxide Solubility, *Inorganic Chemistry*, 1987. 26 (4140-4142)

36. Bundschuh, T., Knopp, R., et al. Application of LIBD to the determination of the solubility of product of thorium(IV)-colloids, *Radiochimica Acta*, 2000. 88 (625-631)

37. Nyquist, R.A. and Kagel, R.O. **Infrared Spectra of Inorganic Compounds, Vol. 4: The Handbook of Infrared ans Raman Spectra of Inorganic Compounds and Organic Salts**, Academic Press Inc, London 1997 pp. 230-231

38. Research Information Database, National Institute of Advanced Industrial Science and Technology, Japan. http://www.aist.go.jp/RIODB/riohomee.html

39. Neck, V. and Kim, J.L. Solubility and Hydrolysis of Tetravalent Actinides, *Radiochimica Acta*, 2001. 89 (1-16)

Appendix A: Solubility Data

A.1 ICP-MS Data

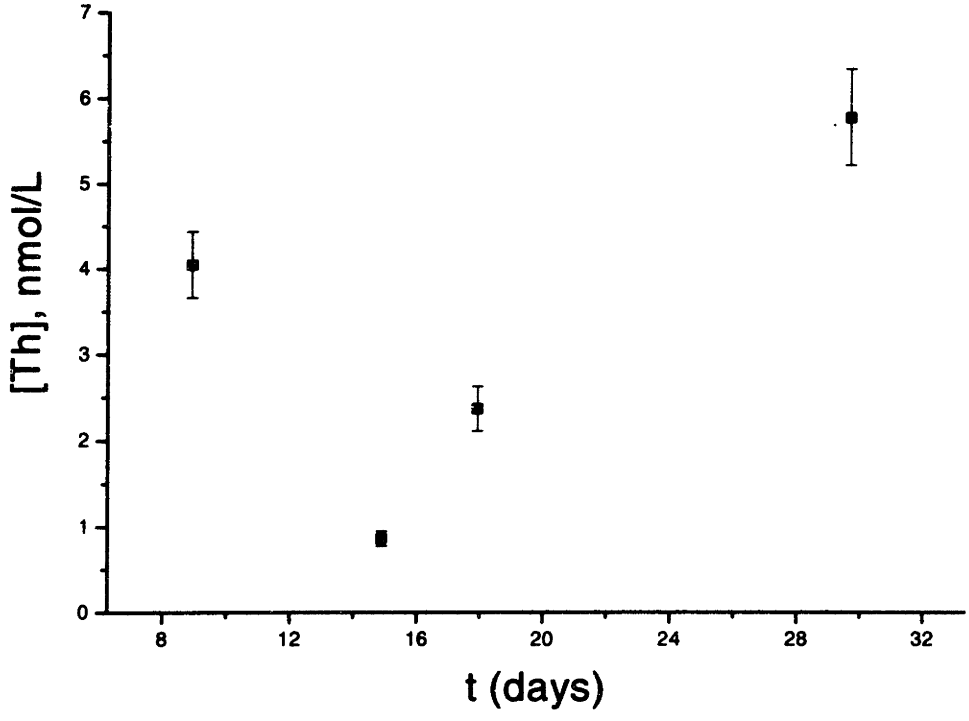

Figure A.1 pH = 6.40, 100% Ar

Appendix B: Unfiltered Samples

Data for unfiltered samples and the corresponding filtered samples are in the tables below. Unfiltered samples are in green.

Time	[Th], mol/L	±
214.1	2.37E-06	4.63E-07
214.4	2.30E-06	4.48E-07
430.2	2.48E-06	4.03E-07
430.5	2.56E-06	4.17E-07
648.2	3.48E-06	2.15E-07
648.4	3.85E-06	2.37E-07

Table B.1 Unfiltered comparison, pH = 2.07, 100% Argon

time	[Th], mol/L	±
214.1	2.34E-06	4.56E-07
214.4	2.18E-06	4.26E-07
430.2	2.40E-06	3.90E-07
430.5	2.51E-06	4.08E-07
648.2	3.78E-06	2.33E-07
648.4	3.69E-06	2.28E-07

Table B.2 Unfiltered comparison, pH = 2.57, 100% Argon

time	[Th], mol/L	±
214.1	1.84E-06	3.59E-07
214.4	1.83E-06	3.58E-07
430.2	1.75E-06	2.85E-07
430.5	1.80E-06	2.93E-07
648.2	2.75E-06	1.70E-07
648.4	2.72E-06	1.68E-07

Table B.3 Unfiltered comparison, pH = 2.99, 100% Argon

time	[Th], mol/L	±
436	7.28E-06	1.87E-06
436	7.42E-06	1.90E-06
646	8.52E-06	2.18E-06
646	8.54E-06	2.19E-06

Table B.4 Unfiltered comparison, pH = 2.06, 10% CO_2

time	[Th], mol/L	±
436	1.57E-06	4.017E-07
436	1.66E-06	4.25E-07
646	2.00E-06	5.13E-07
646	2.03E-06	5.19E-07

Table B.5 Unfiltered comparison, pH = 2.57, 10% CO_2

time	[Th], mol/L	±
216.17	3.87E-08	2.06E-08
216.17	2.664E-08	1.41E-08
436	2.12E-08	1.13E-08
436	1.37E-08	7.30E-09
646	4.64E-08	2.47E-08
646	3.27E-08	1.73E-08

Table B.6 Unfiltered comparison, pH = 3.10, 10% CO_2

time	[Th], mol/L	±
216.17	3.74E-08	7.72E-09
216.17	4.24E-08	8.75E-09
436	5.23E-08	1.08E-08
436	3.64E-08	7.52E-09
646	7.35E-08	1.52E-08
646	2.02E-08	4.16E-09

Table B.7 Unfiltered comparison, pH = 3.60, 10% CO_2

time	[Th], mol/L	±
216.17	6.88E-08	2.32E-08
216.17	4.71E-08	1.59E-08
436	1.71E-08	5.76E-09
436	4.29E-08	1.44E-08
646	6.85E-08	2.31E-08
646	6.66E-08	2.24E-08

Table B.8 Unfiltered comparison, pH = 4.13, 10% CO_2

time	[Th], mol/L	±
216.17	3.39E-08	2.28E-08
216.17	3.58E-08	2.41E-08
436	3.27E-08	2.21E-08
436	2.87E-08	1.93E-08
646	1.17E-07	7.87E-08
646	1.80E-07	1.21E-07

Table B.9 Unfiltered comparison, pH = 4.48, 10% CO_2

time	[Th], mol/L	±
216.17	4.48E-08	4.70E-08
216.17	4.54E-08	4.76E-08
436	2.08E-08	2.18E-08
436	3.45E-08	3.62E-08
646	1.12E-07	1.18E-07
646	5.05E-08	5.30E-08

Table B.10 Unfiltered comparison, pH = 5.05, 10% CO_2

time	[Th], mol/L	±
216	2.87072E-07	1.71107E-07
216	7.10043E-08	4.23215E-08
431.28	4.96549E-08	2.95964E-08
431.28	5.52723E-08	3.29446E-08
815.088	1.08382E-07	6.46002E-08
815.088	1.13757E-07	6.78036E-08

Table B.11 Unfiltered comparison, pH = 5.51, 10% CO_2

216	**6.46E-08**	**3.68E-08**
216	4.07E-08	2.32E-08
431.28	**4.61E-08**	**2.62E-08**
431.28	3.13E-07	1.78E-07
815.088	**1.90E-08**	**1.08E-08**
815.088	3.60E-08	2.05E-08

Table B.12 Unfiltered comparison, pH = 6.03, 10% CO_2

time	[Th], mol/L	±
9	**9.32E-08**	**2.957E-08**
9	9.78E-08	3.10E-08
17.97	**1.89E-08**	**5.98E-09**
17.97	4.36E-06	1.38E-08
33.962	**3.71E-08**	**1.18E-08**
33.962	1.34E-07	4.26E-08

Table B.13 Unfiltered comparison, pH = 6.48, 10% CO_2

Appendix C: XRD Scans

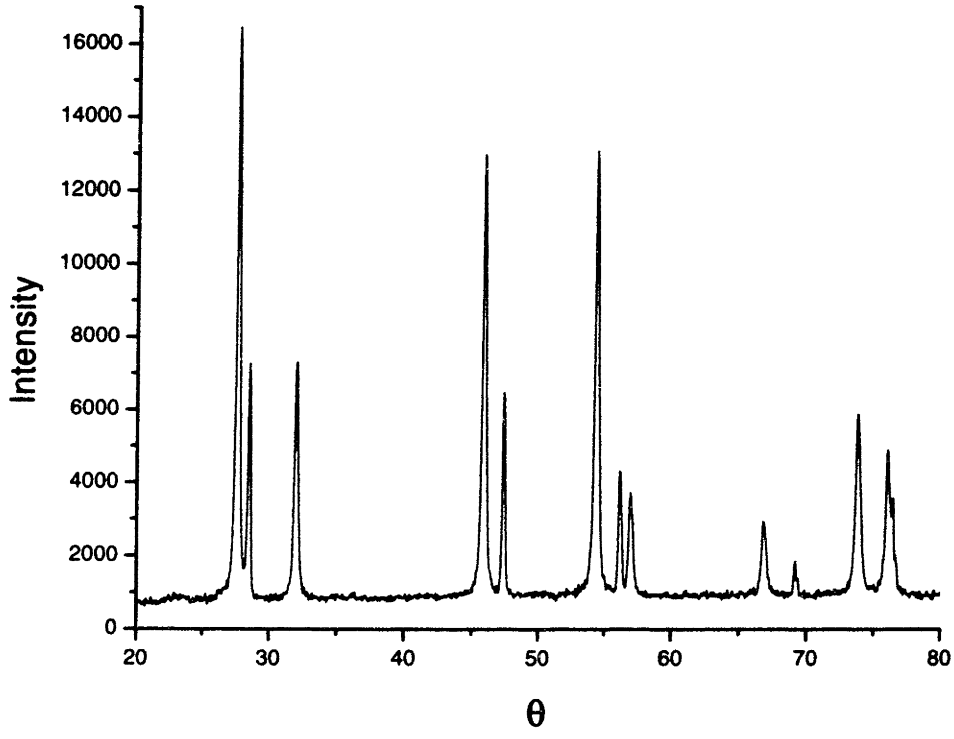

Figure C.1 XRD pattern for pH = 2.07, 100% Argon

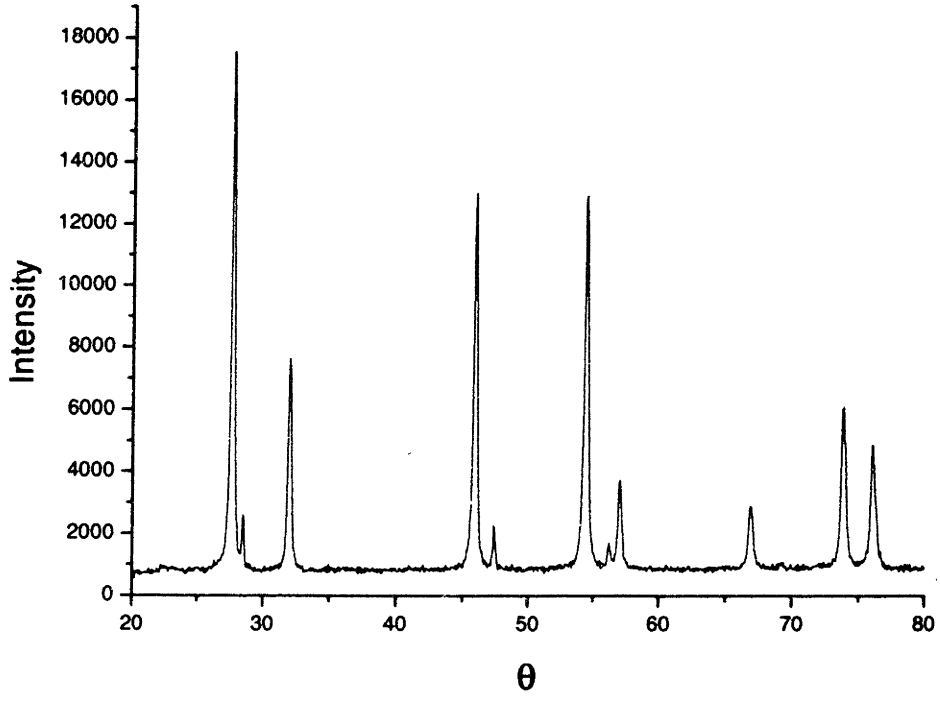

Figure C.2 XRD pattern for pH = 2.99, 100% Argon

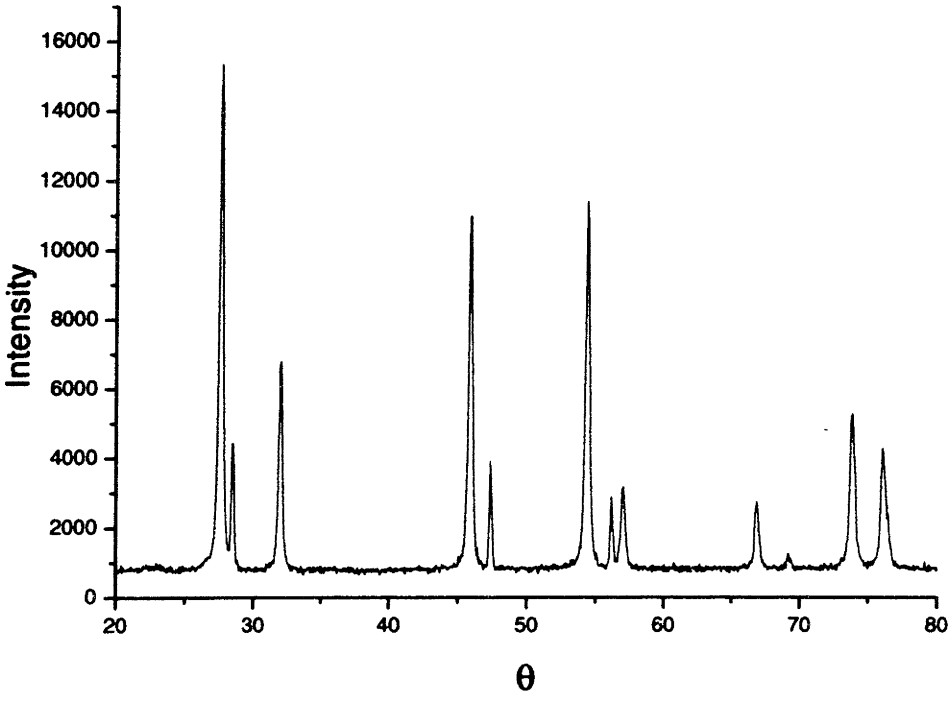

Figure C.3 XRD pattern for pH = 4.27, 100% Argon

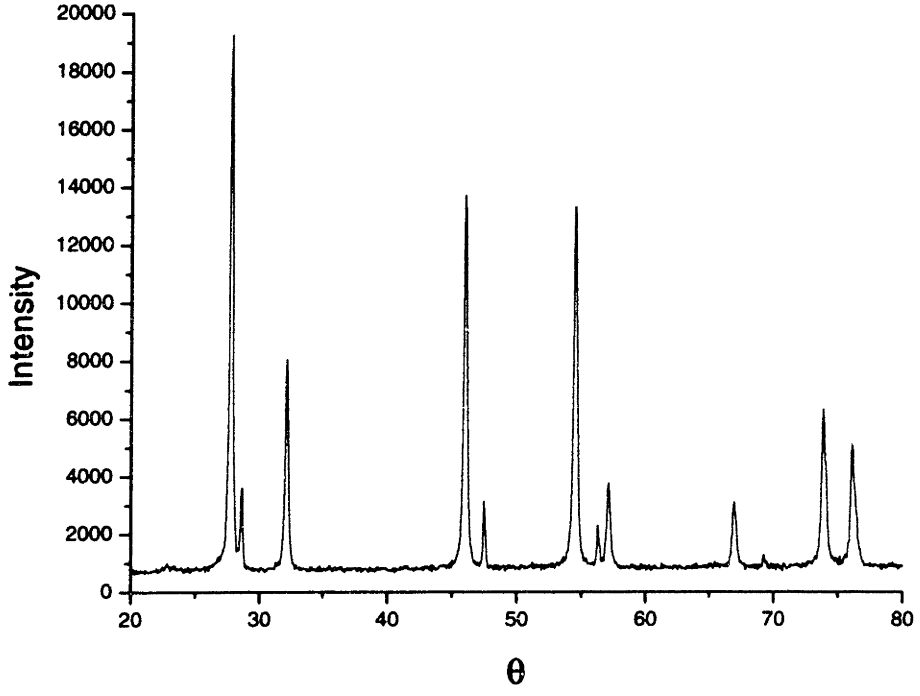

Figure C.4 XRD patttern for pH = 5.84, 100% Argon

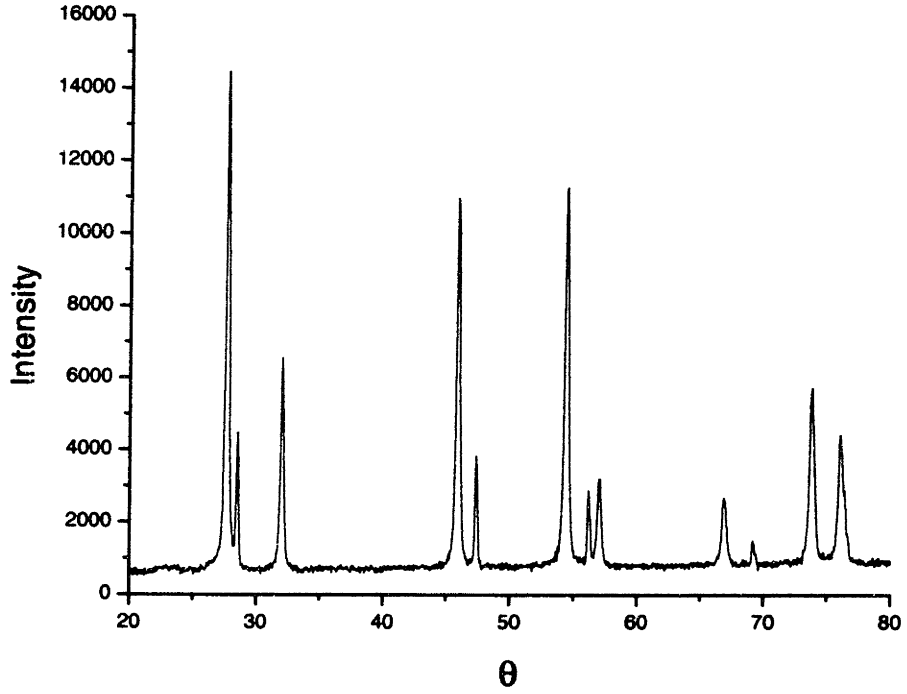

Figure C.5 XRD pattern for pH = 6.90, 100% Argon

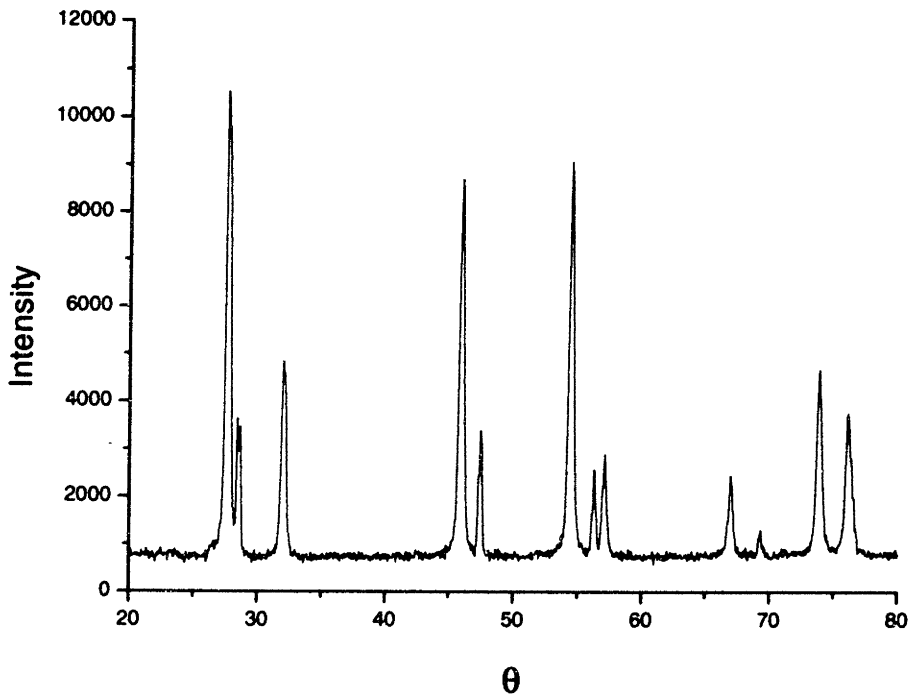

Figure C.6 XRD pattern for pH = 8.08, 100% Argon

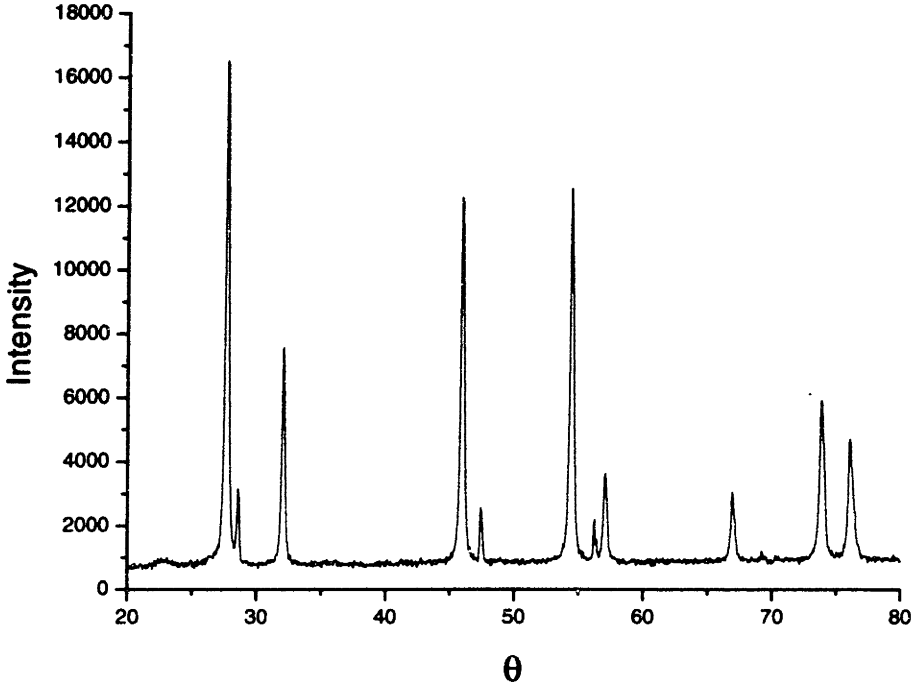

Figure C.7 XRD pattern for pH = 8.96, 100% Argon

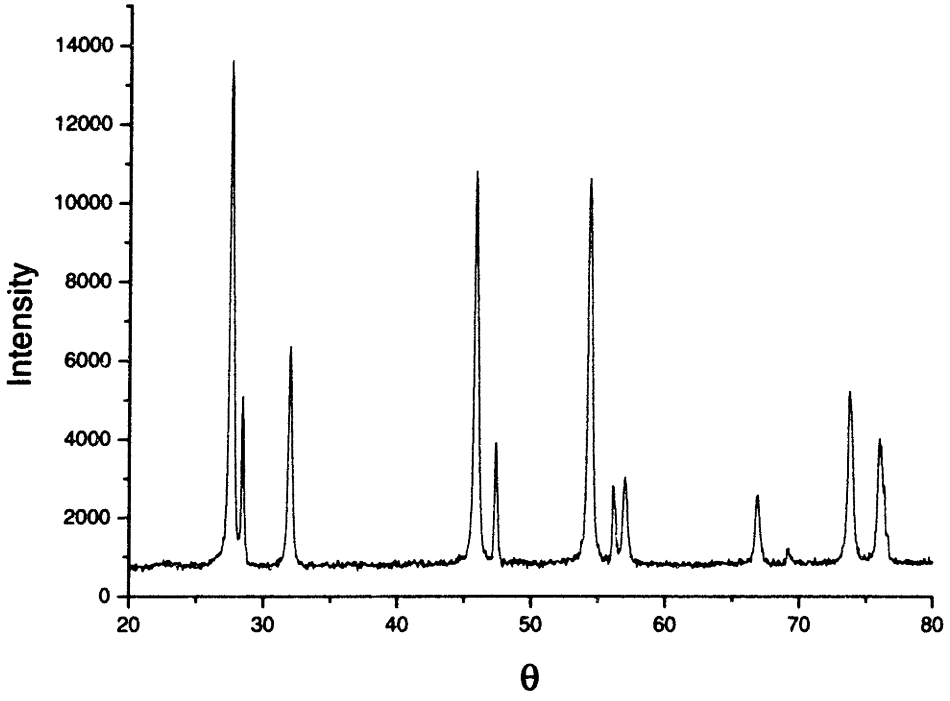

Figure C.8 XRD pattern for pH = 10.07, 100% Argon

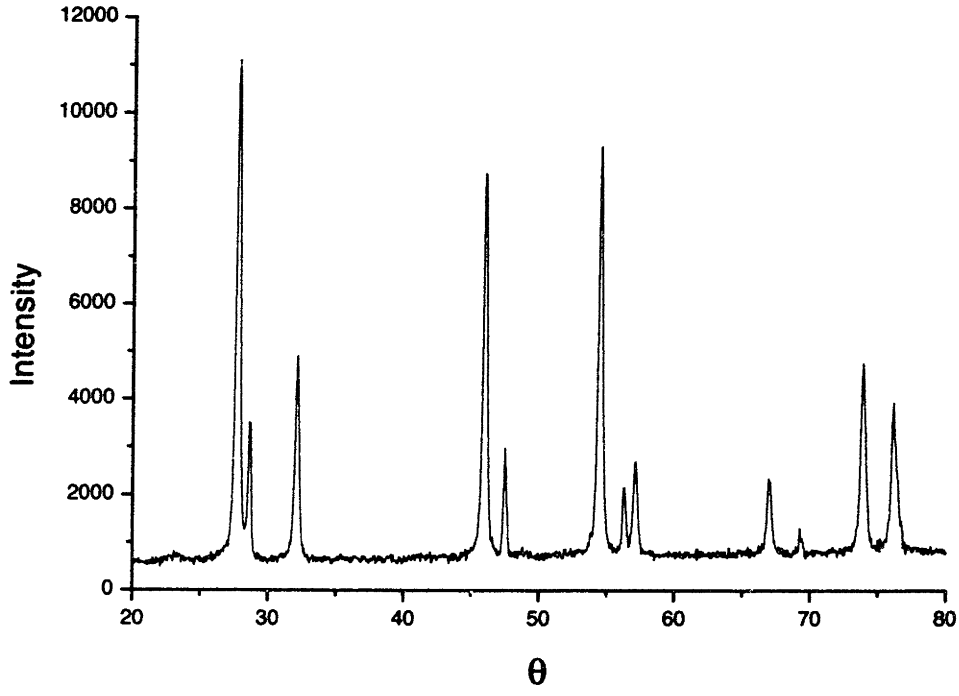

Figure C.9 XRD pattern for pH = 11.08, 100% Argon

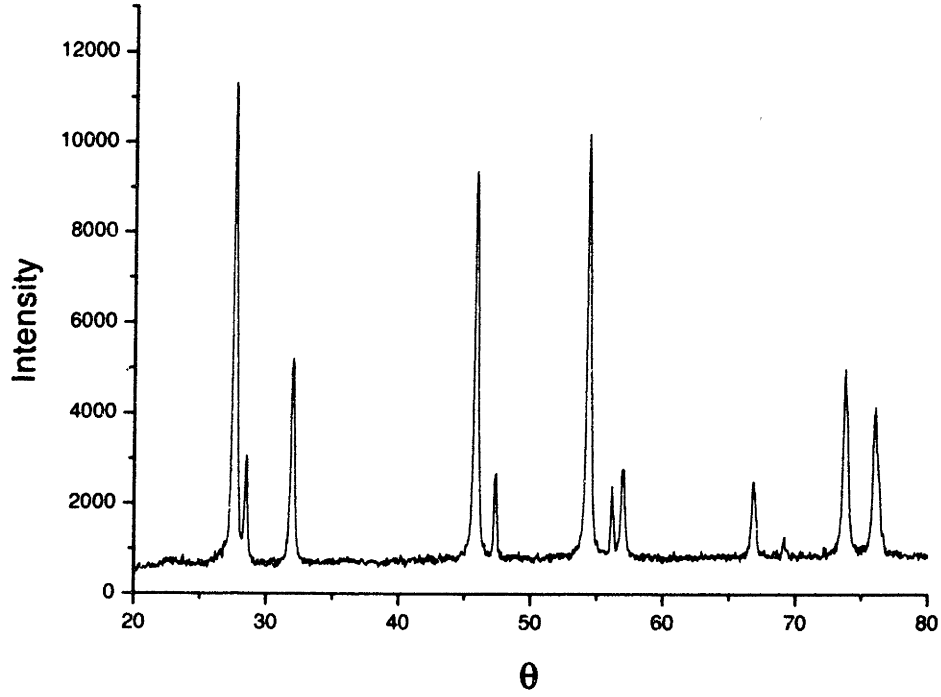

Figure C.10 XRD pattern for pH = 2.06, 10% CO_2

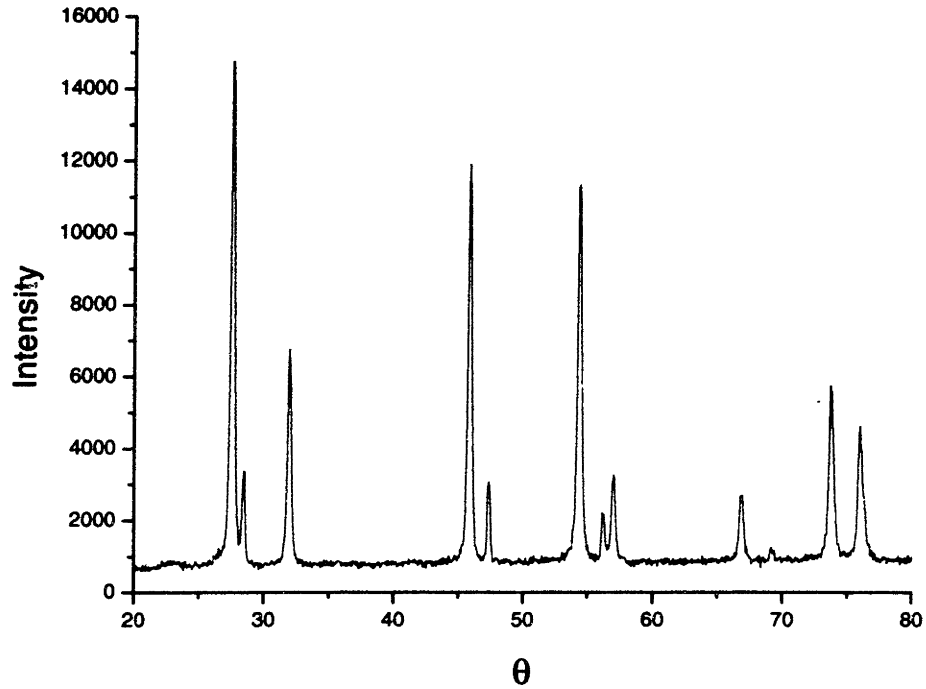

Figure C.11 XRD pattern for pH = 2.57, 10% CO_2

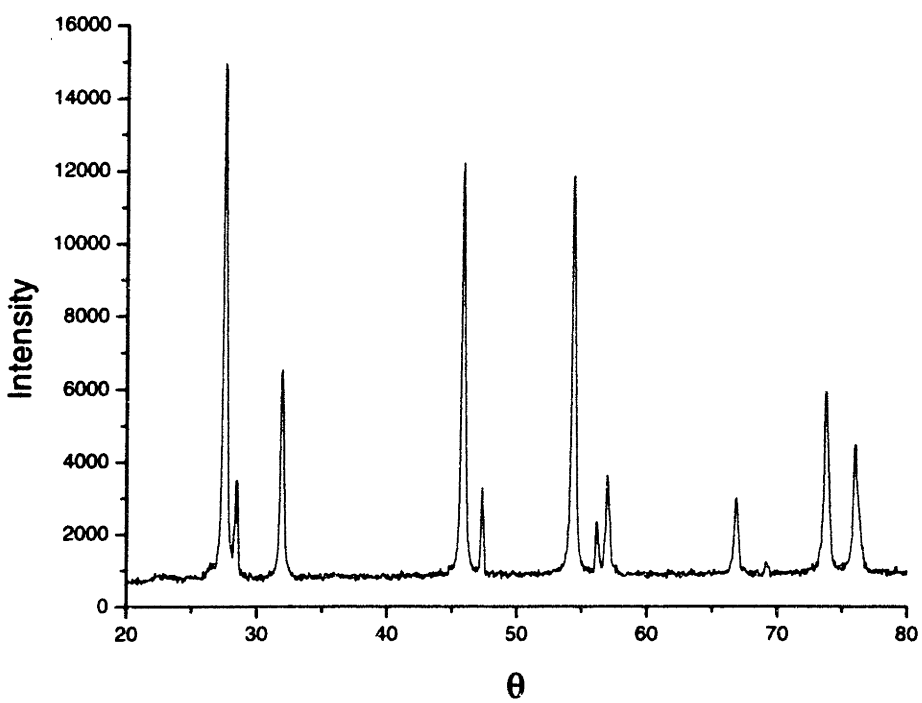

Figure C.12 XRD pattern for pH = 3.10, 10% CO_2

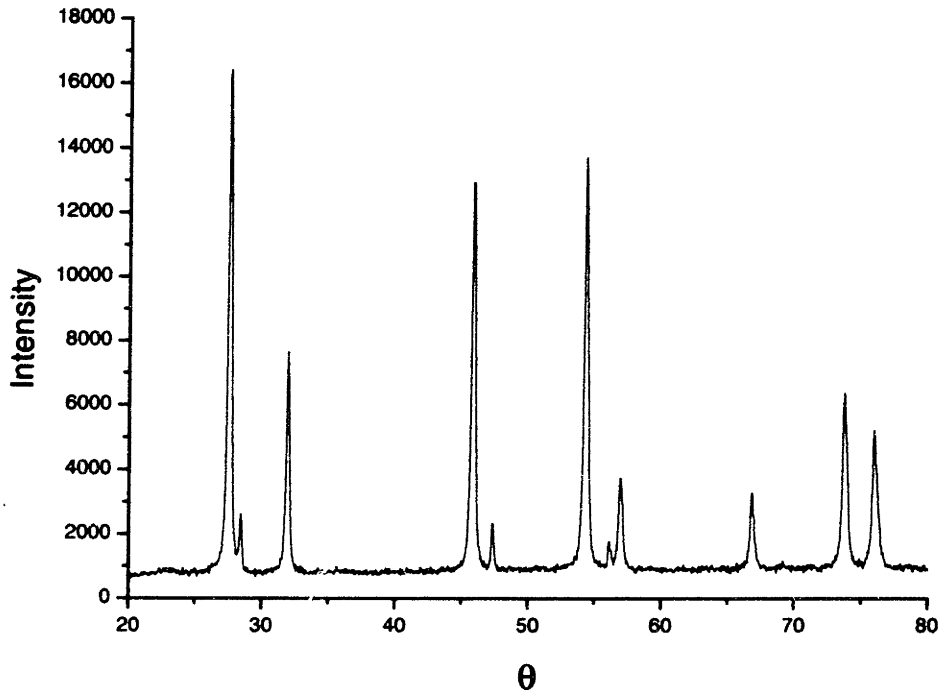

Figure C.13 XRD pattern for pH = 3.60, 10% CO_2

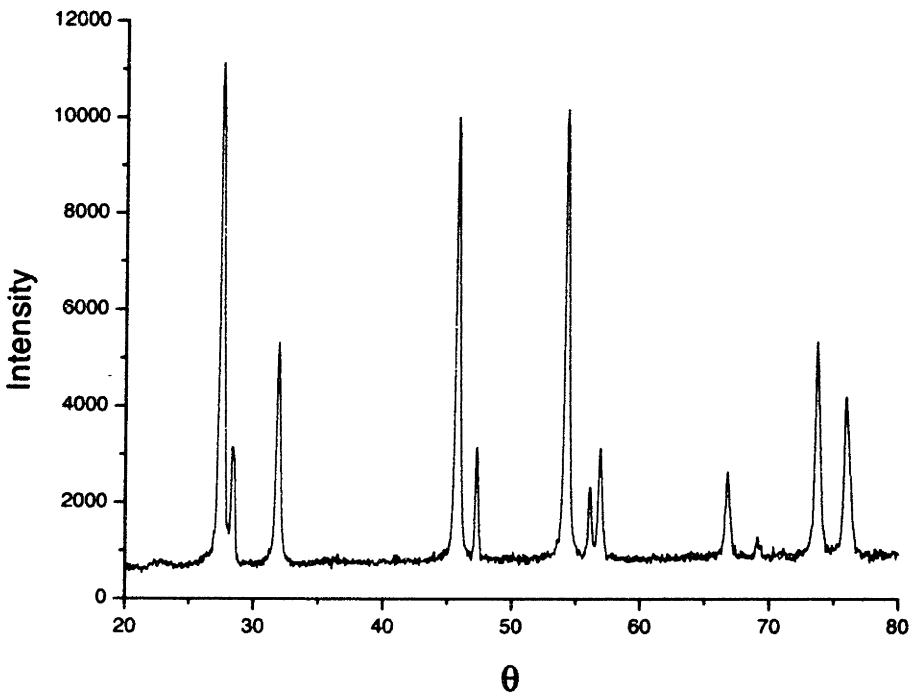

Figure C.14 XRD pattern for pH = 4.13, 10% CO_2

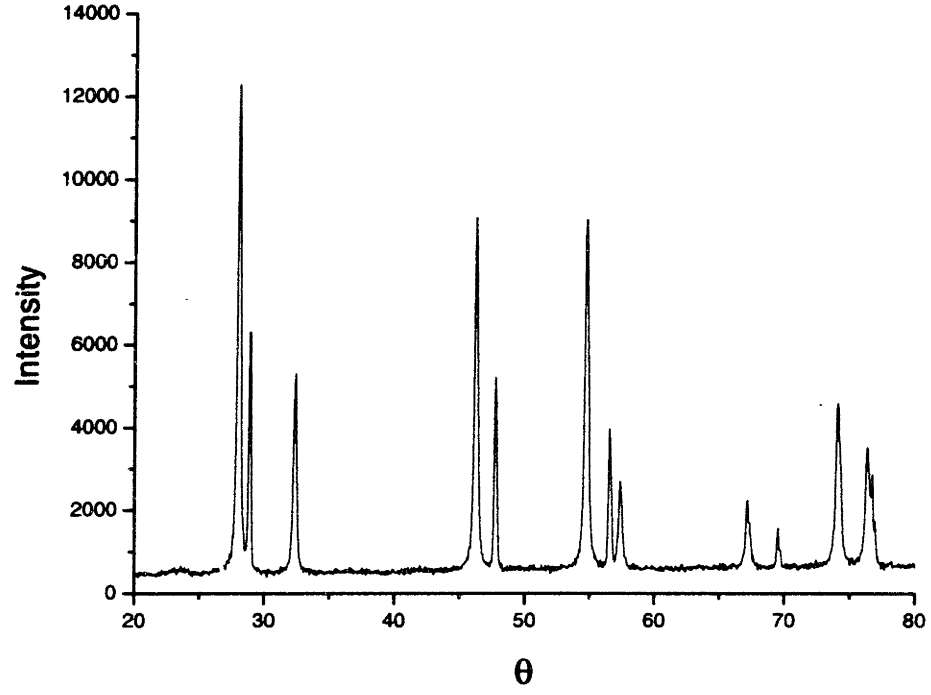

Figure C.15 XRD pattern for pH = 4.48, 10% CO_2

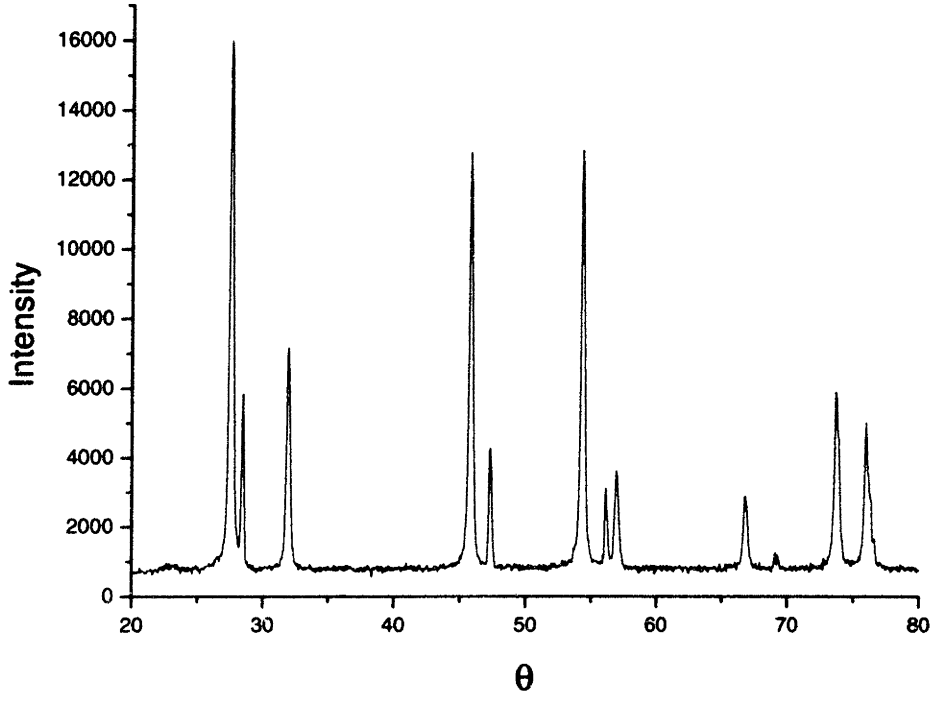

Figure C.16 XRD pattern for pH = 5.05, 10% CO_2

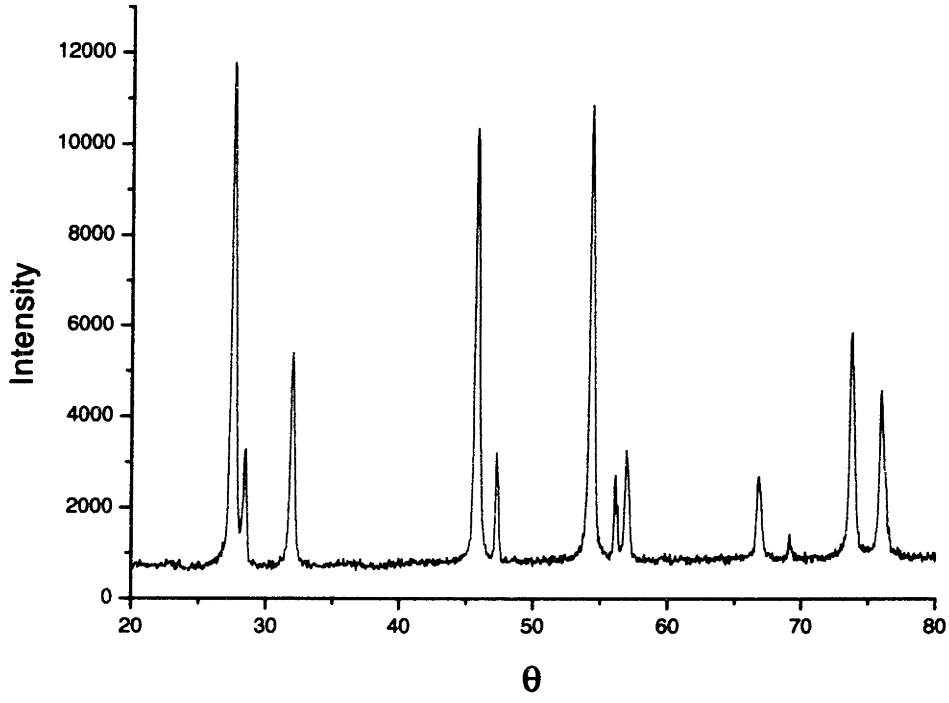

Figure C.17 XRD pattern for pH = 5.51, 10% CO_2

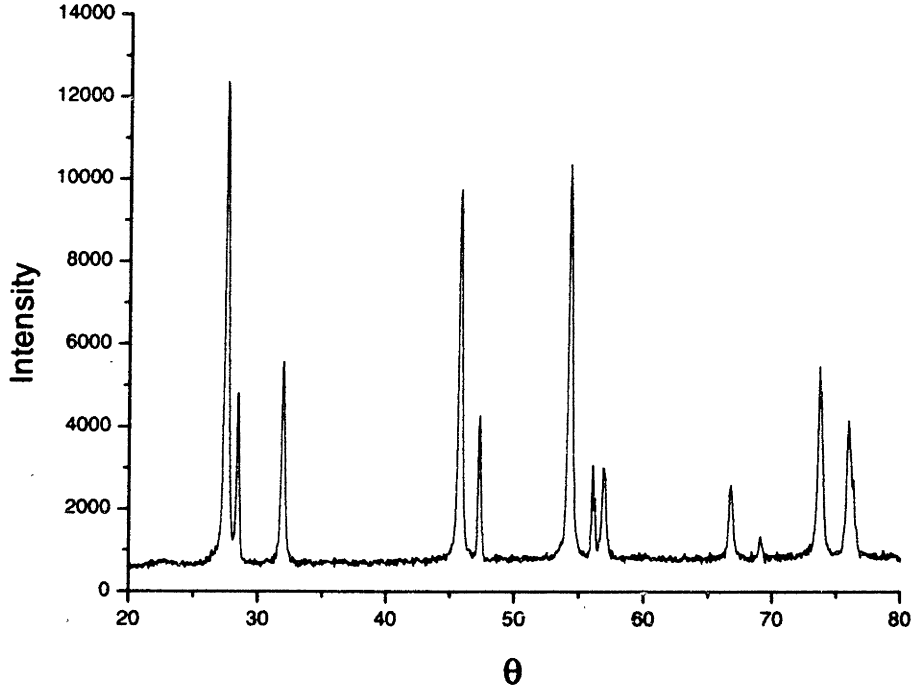

Figure C.18 XRD pattern for pH = 6.03, 10% CO_2

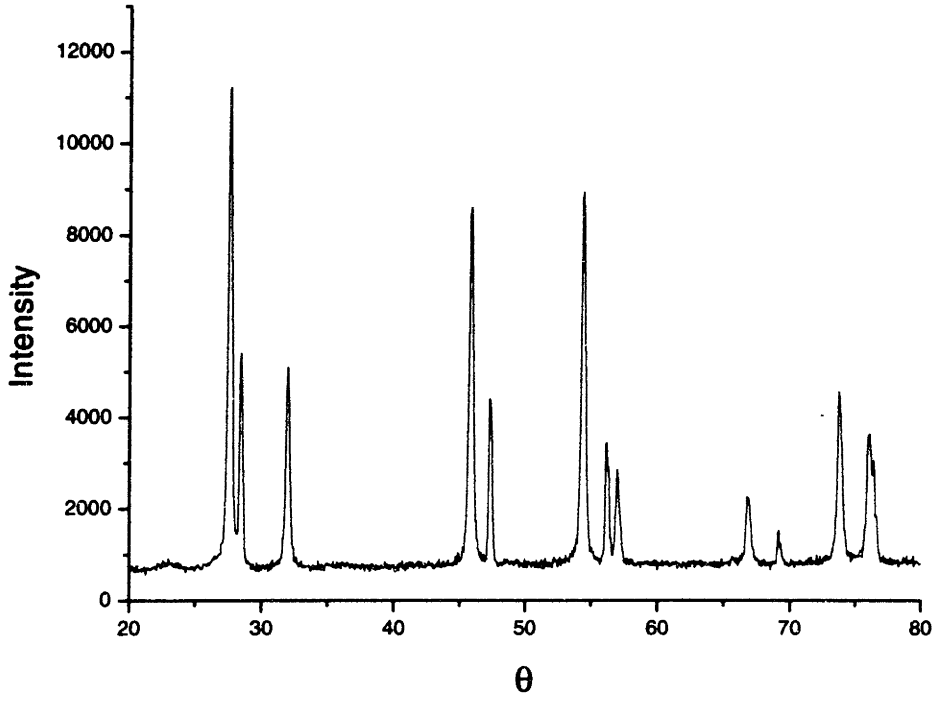

Figure C.19 XRD pattern for pH = 6.48, 10% CO_2

Appendix D: FTIR Spectra

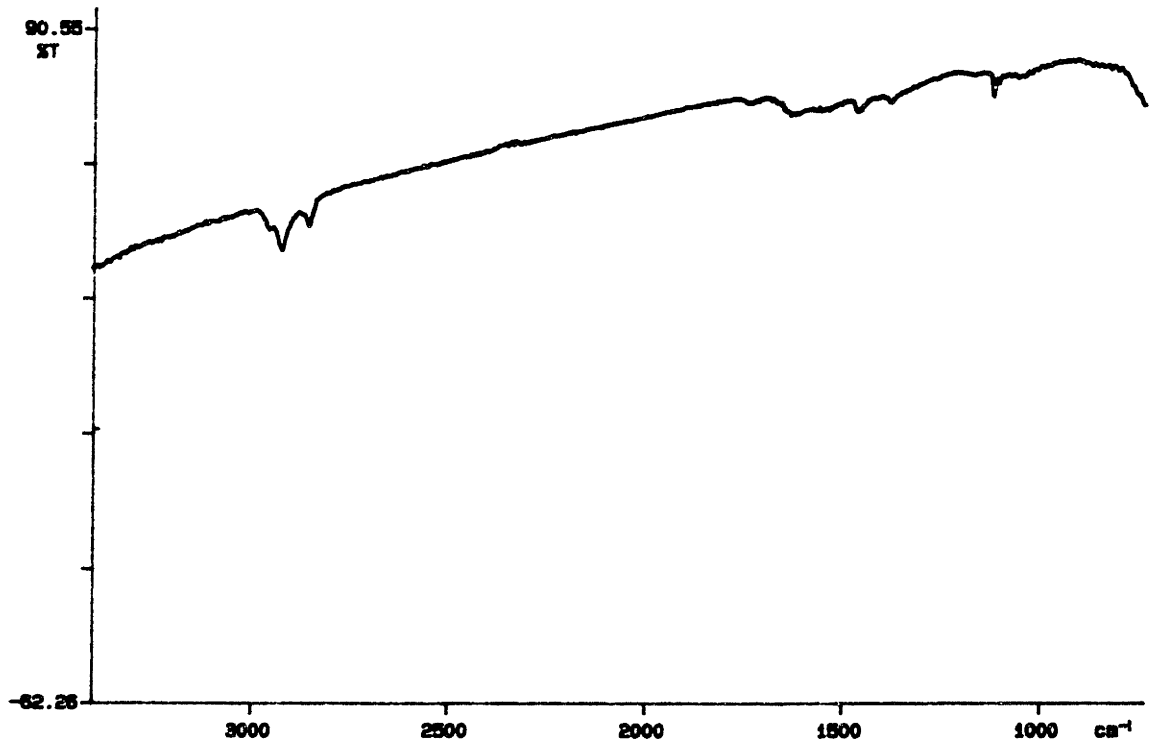

Figure D.1 FTIR Spectrum for pH = 3.68, 100% argon

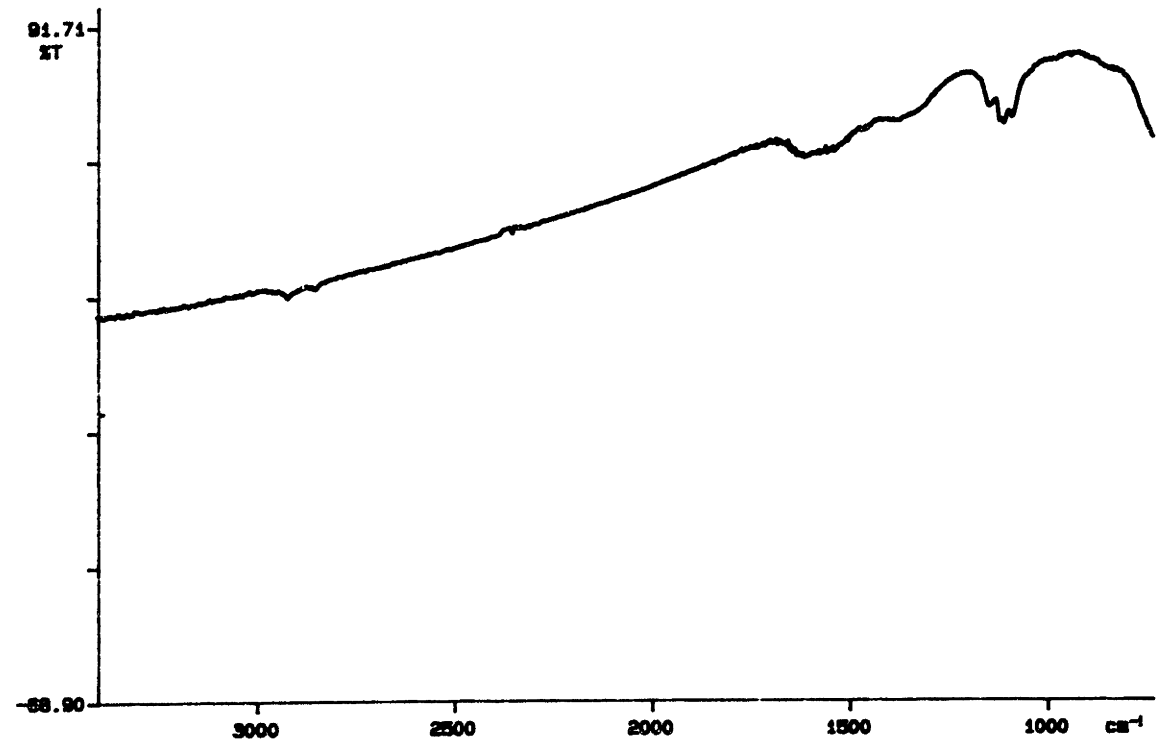

Figure D.2 FTIR spectrum for pH = 6.40, 100% argon

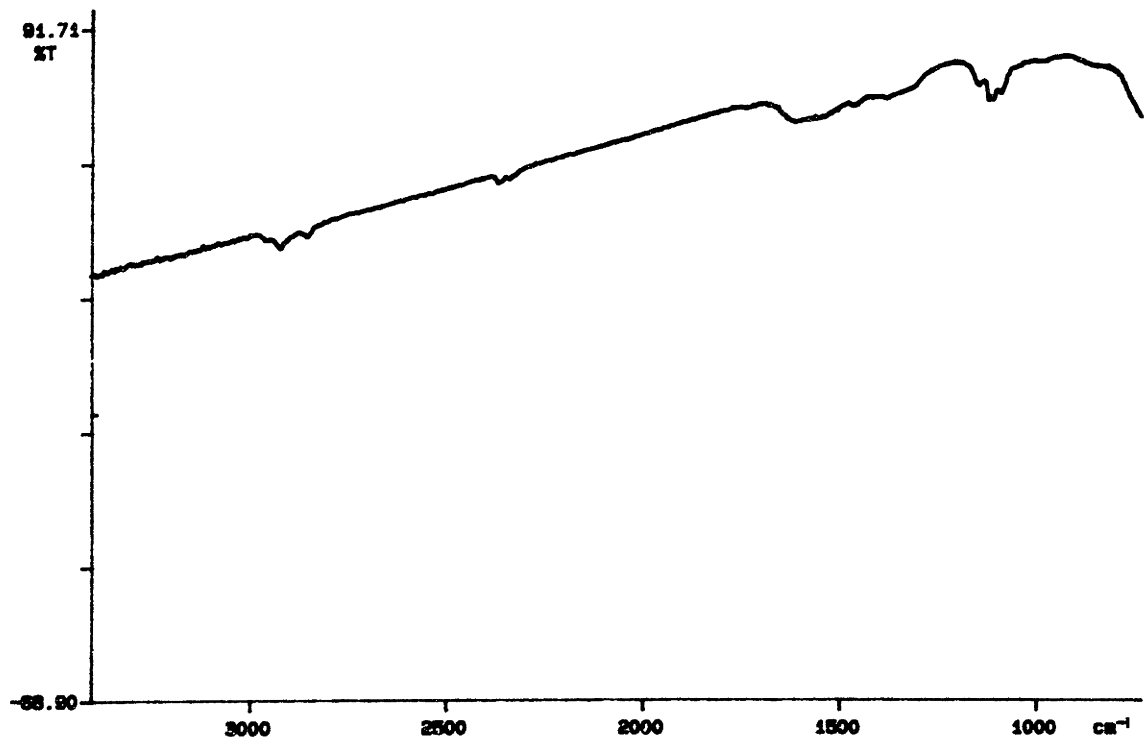

Figure D.3 FTIR spectrum for pH = 8.96, 100% argon

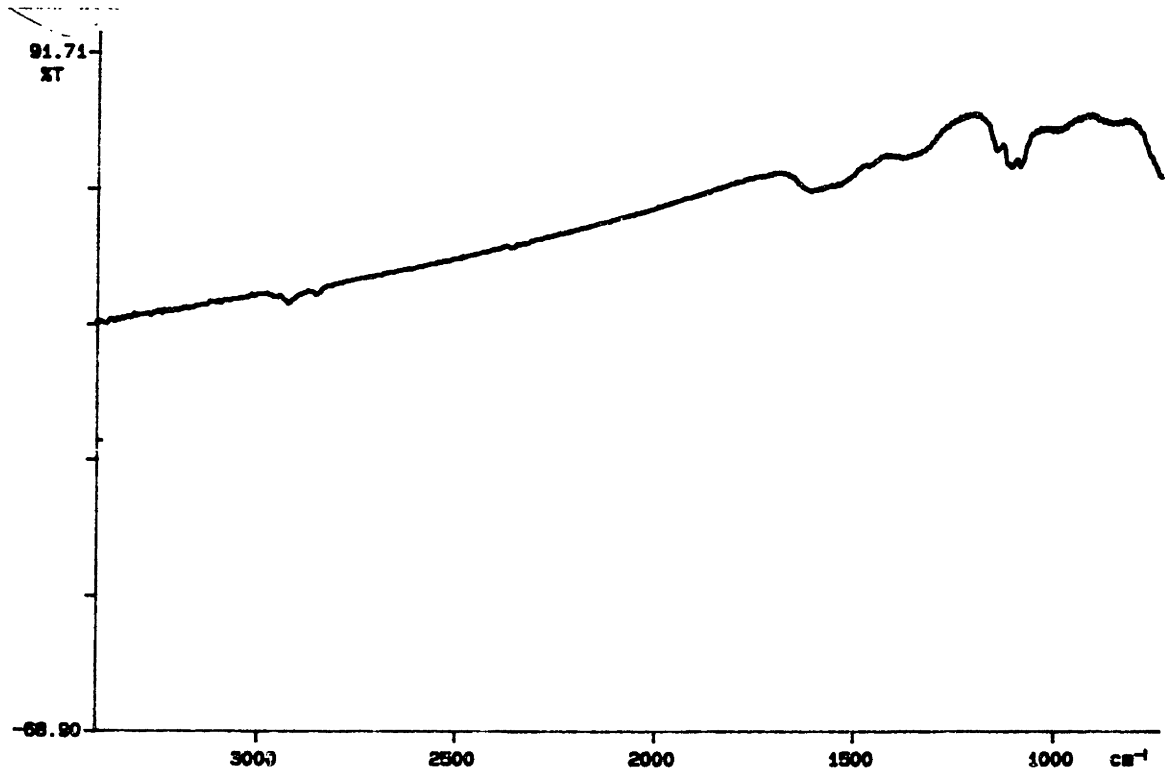

Figure D.4 FTIR spectrum for pH = 11.55, 100% argon

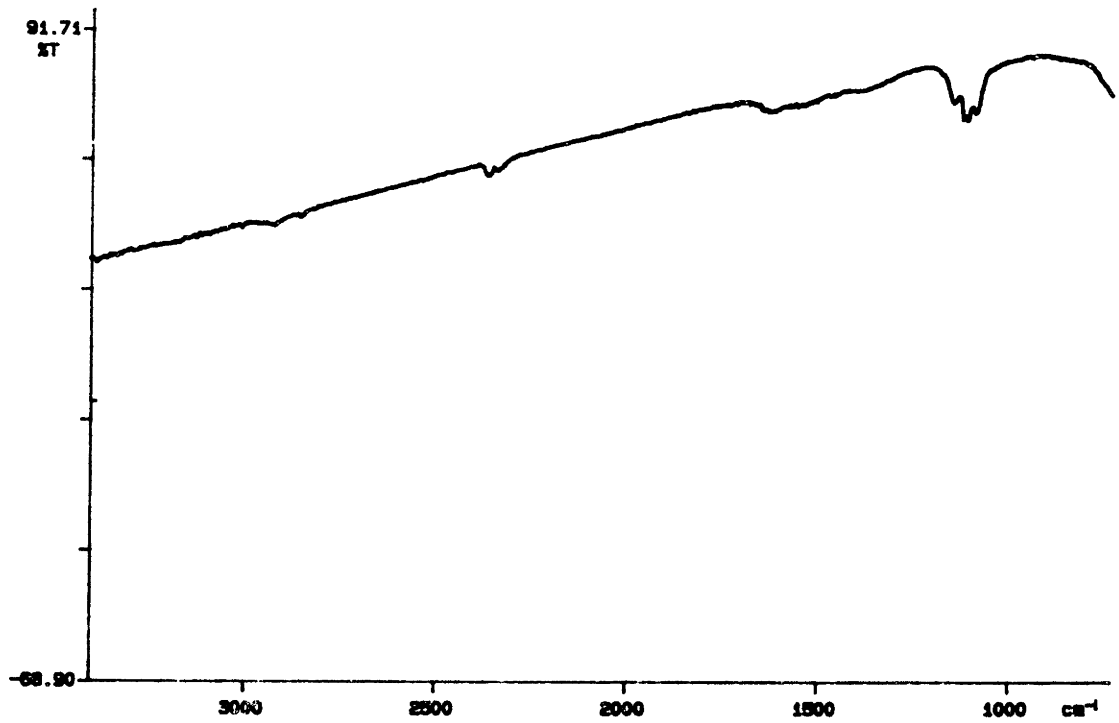

Figure D.5 FTIR spectrum for pH = 2.06, 10% CO_2

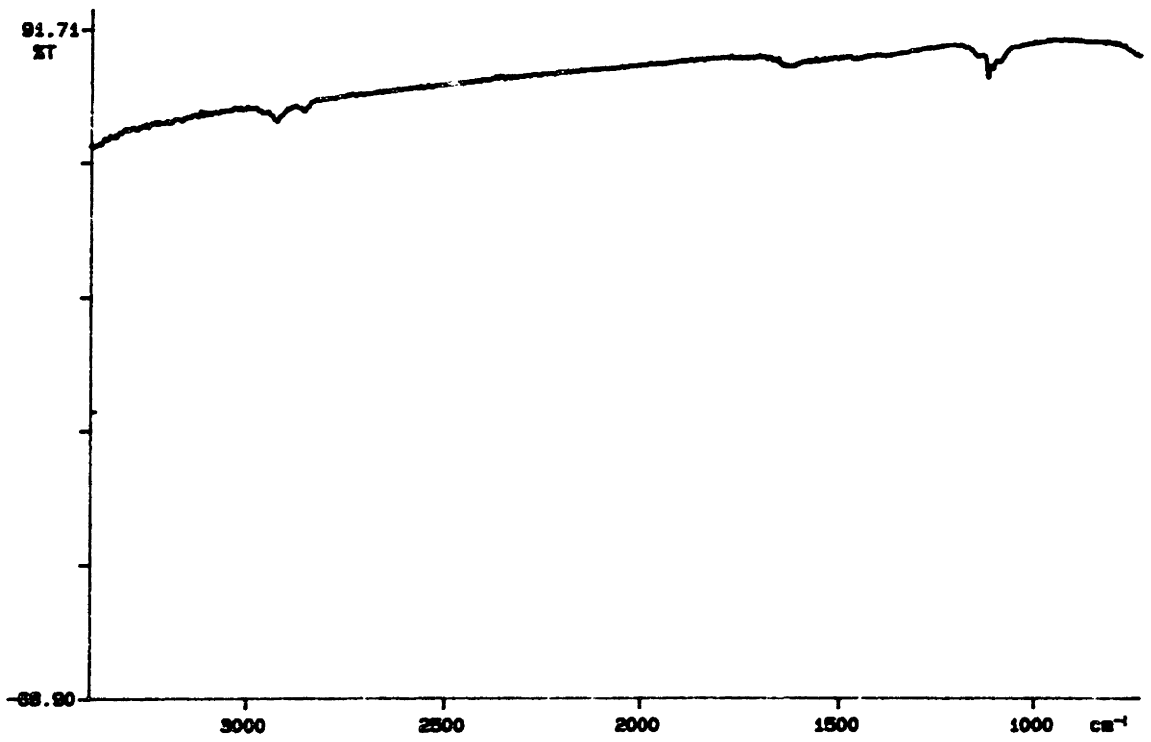

Figure D.6 FTIR spectrum for pH = 3.60, 10% CO_2

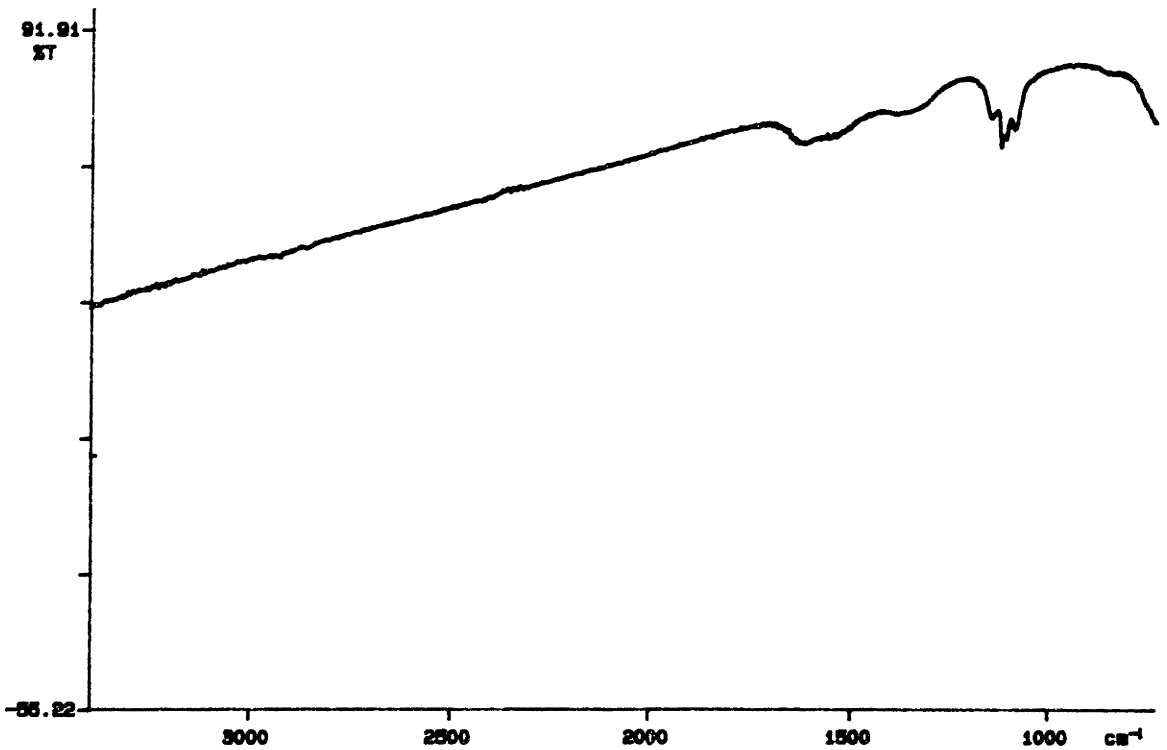

Figure D.7 FTIR spectrum pH = 5.05, 10% CO_2

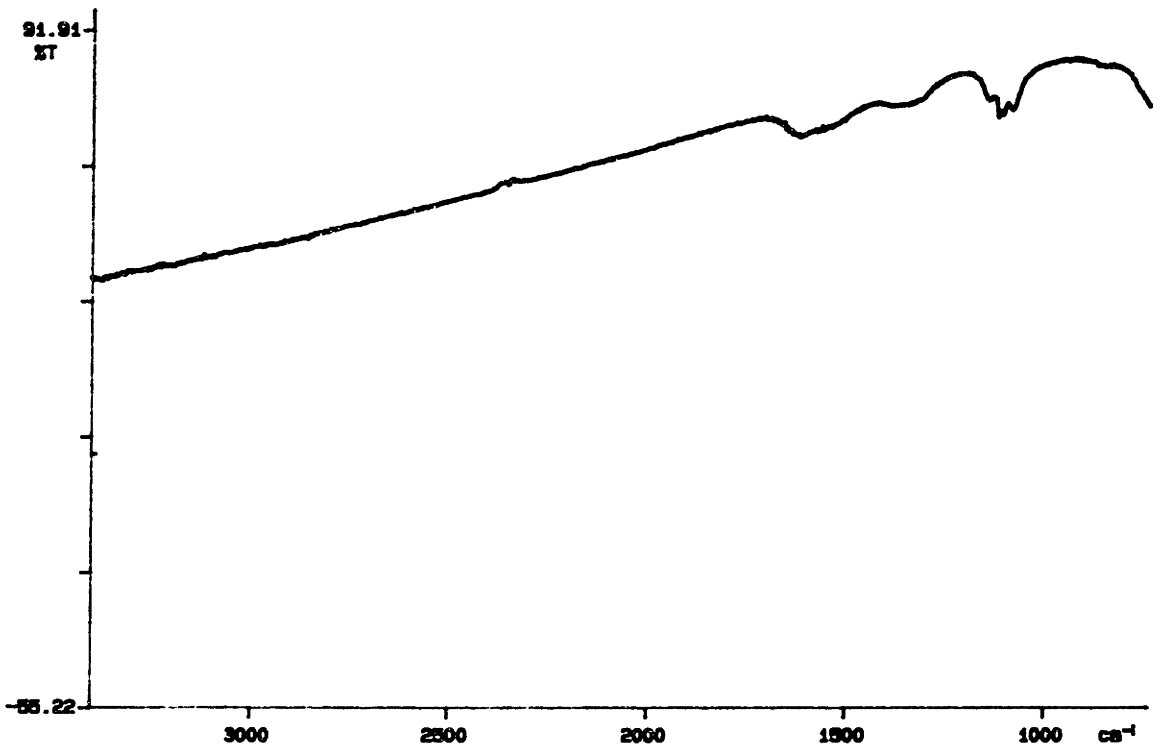

Figure D.8 FTIR spectrum for pH = 6.48, 10% CO_2

Appendix E: Thoria Stabilization of Urania

E.1 Speciation Modelling

The impact of thoria on urania solubility was modeled using the hydro-geochemical equilibrium code CHESS. Modeling was performed with J-13 groundwater from the proposed Yucca Mountain Waste Repository site, Nevada at an Eh of 700 mV and pH 6 through 9. J-13 water's composition was characterized by Ogard et al. as given below:

Cations	Concentration [mM]	Anions	Concentration [mM]
Na[+]	1.96	F[-]	0.11
K[+]	0.136	Cl[-]	0.18
Li[+]	0.009	NO3[-]	0.16
Ca[2+]	0.29	SO4[2-]	0.19
Mg[2+]	0.072	Quartz	1.07
Mn[2+]	0.00002	Total Carbonate	2.81
Fe[3+]	0.0008		
Al[3+]	0.001	PH	7
		Eh	700 mV

Table E.1: Characterization of Yucca Mountain J-13 water

The solubility of UO_2 was modeled using Yucca Mountain conditions and J-13 ground water at room temperature and 90 °C, which is close to the expected repository temperature. Figures 1 and 2 show the results at 25 °C and 90 °C respectively. At 25 °C the most prominent species is the carbonate species $UO_2(CO_3)^{4-}$, which accounts for the majority of uranium in solution. Species concentrations are in the micromolar range. Figure E.1 shows the UO_2 spectiation at 25 °C.

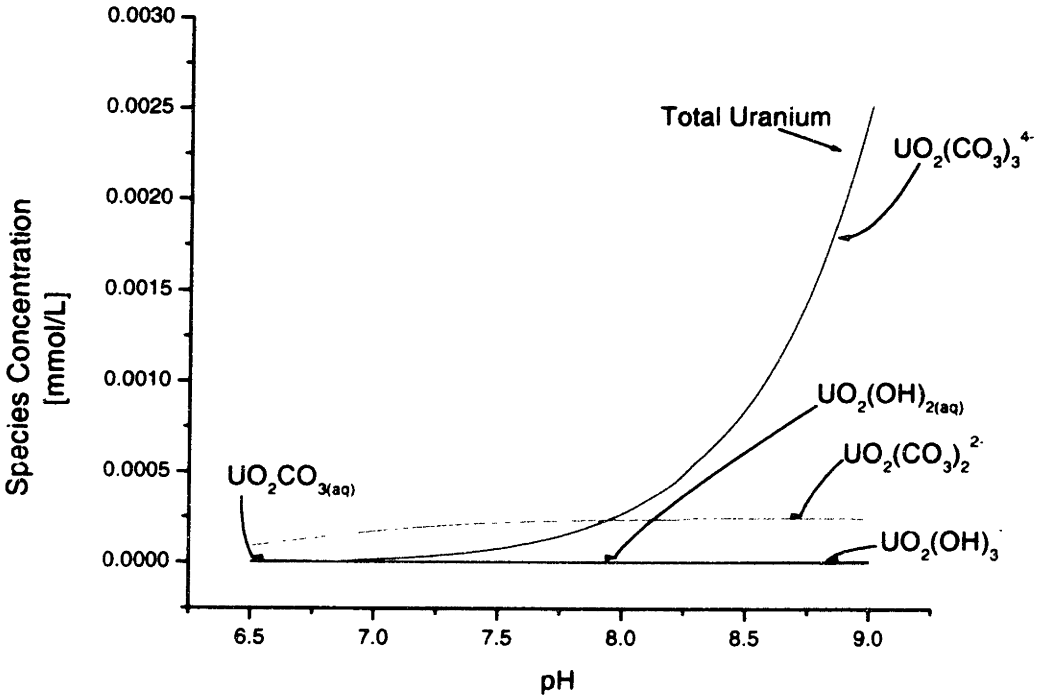

Figure E.1 UO_2 speciation vs. pH, Eh = 300 mV, T = 25 °C

In the higher temperature second case, the dominant species is $CaUO_4$, which builds in rapidly around pH 7 to millimolar levels, two to three orders of magnitude higher than the carbonate species concentrations. Carbonate species concentrations do not change significantly with temperature. This is shown in Figure E.2.

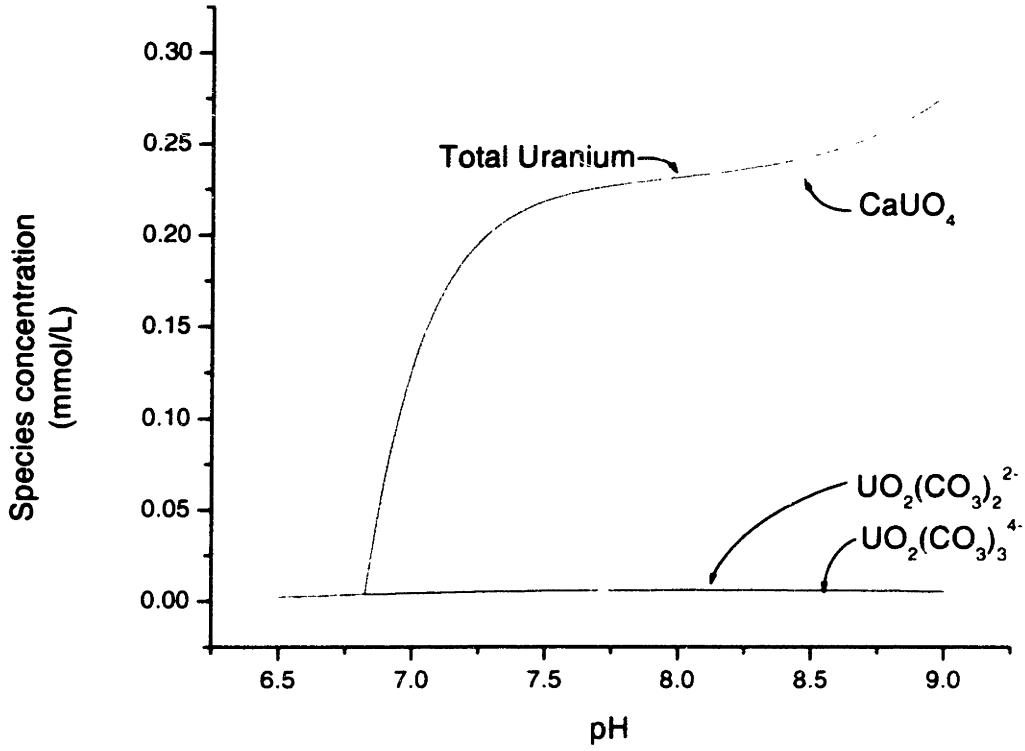

Figure E.2 UO_2 speciation vs. pH, Eh = 700 mV, T = 90 °C

Microheterogeneous fuel will consist of separate urania and thoria pellets. Because of this, the urania phase will not be stabilized by the thoria phase but will oxidize to U_3O_8 instead, similar to conventional reactor fuel. Dissolution of the uranium pellets is modeled as direct dissolution of U_3O_8 in this case. As in the UO_2 case, dissolution was modeled at room temperature and near repository temperature.

Figure E.3 shows the 25 °C case for U_3O_8. The carbonate species $UO_2(CO_3)^{4-}$ remains dominant. In the high temperature case, $CaUO_4$ shows up again as the most important species.

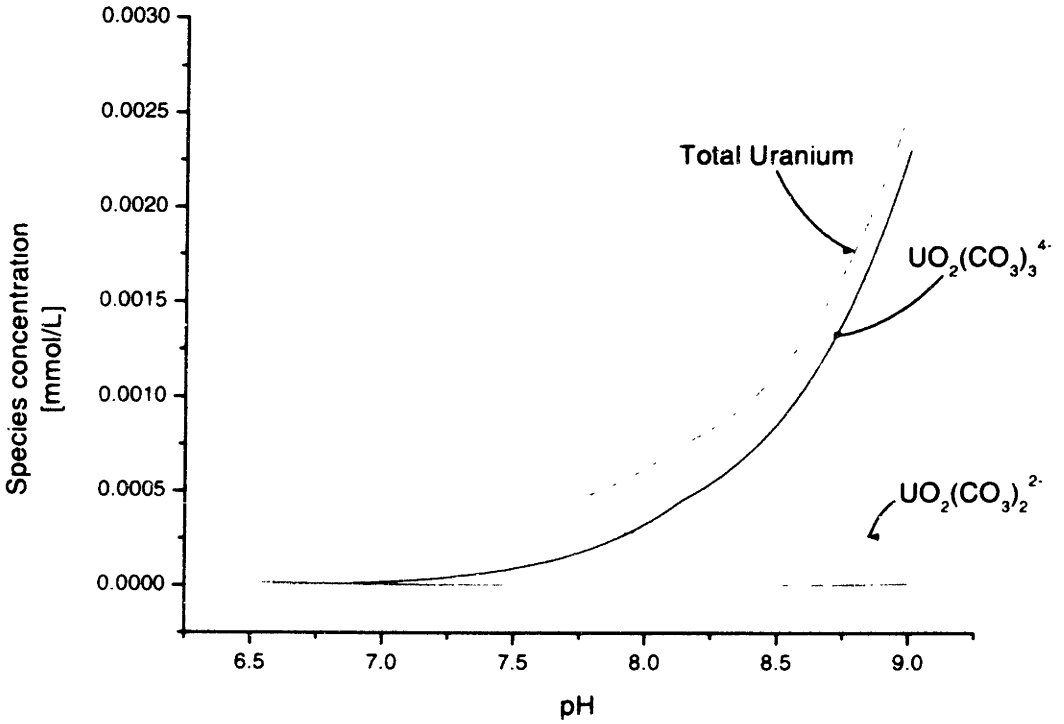

Figure E.3 U_3O_8 specitation vs. pH, Eh = 700 mV, T = 25 °C

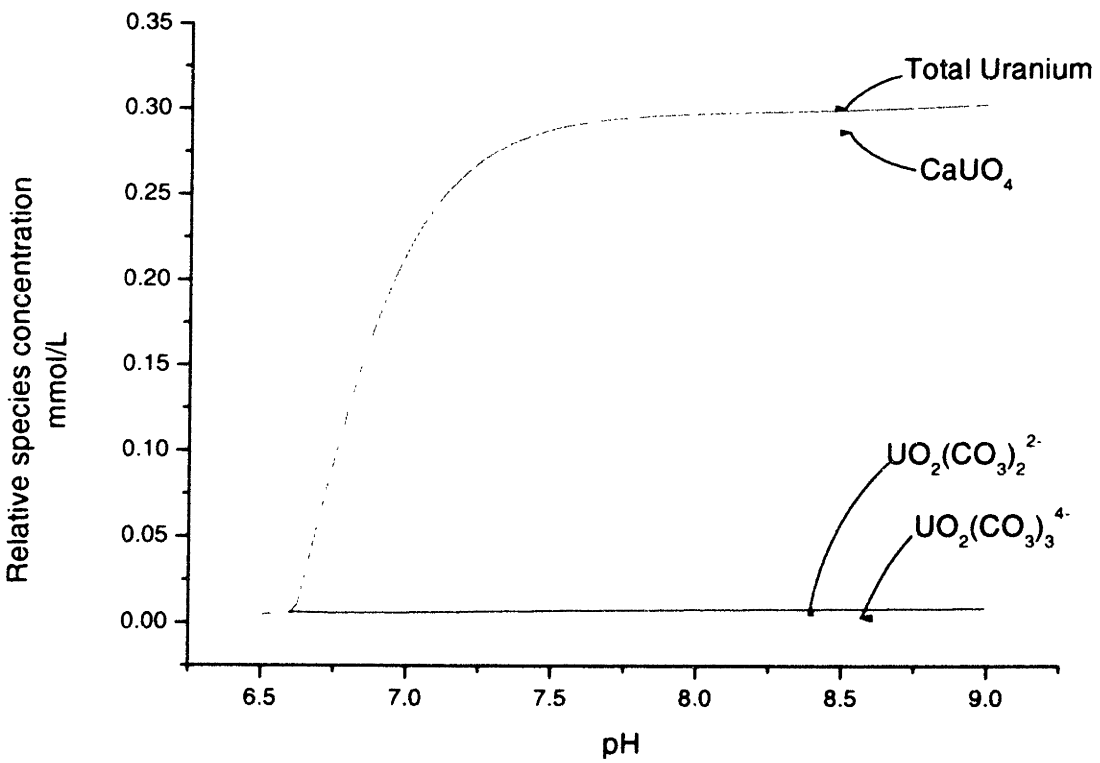

Figure E. 4 U_3O_8 specitation vs. pH, Eh = 700 mV, T = 90 °C

E.2 Comparison

Figures 5 and 6 show the differences in uranium species concentration at room temperature and 90 °C. The difference at room temperature is somewhat small, with a maximum increase of 10% between U_3O_8 and UO_2 dissolution. At the elevated repository temperatures, the amount of dissolved uranium is about 50% higher from the U_3O_8 model than the UO_2 model around neutral pH (7), and decreases to be less than 25% higher by pH 7.5.

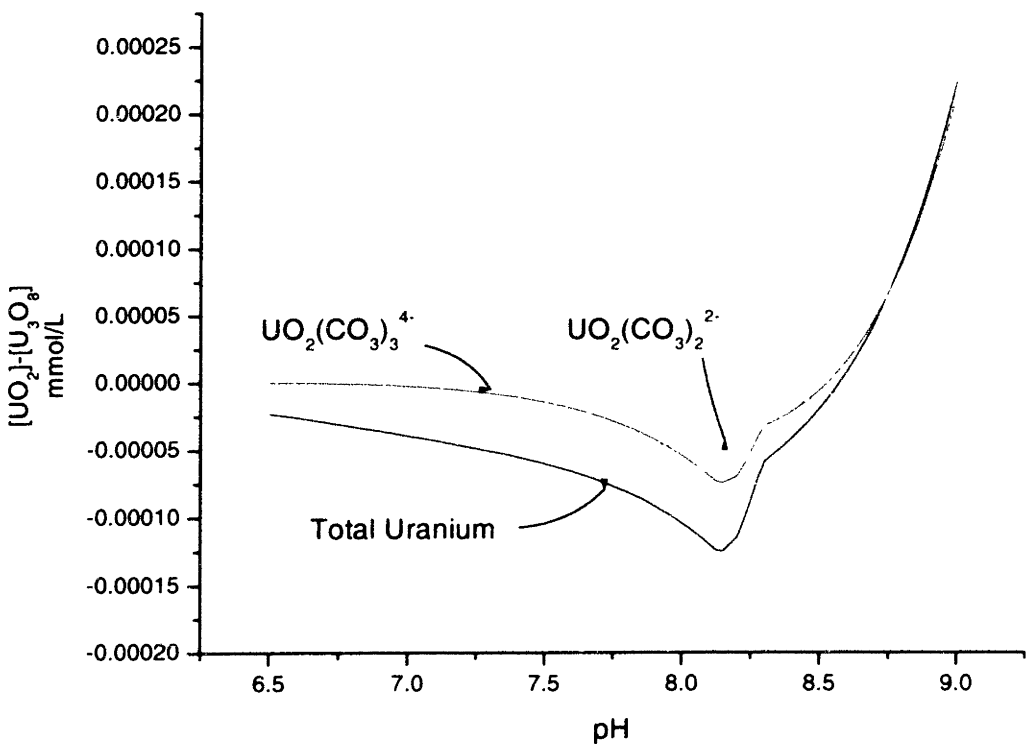

Figure E.5 $[UO_2] - [U_3O_8]$, T = 25 °C

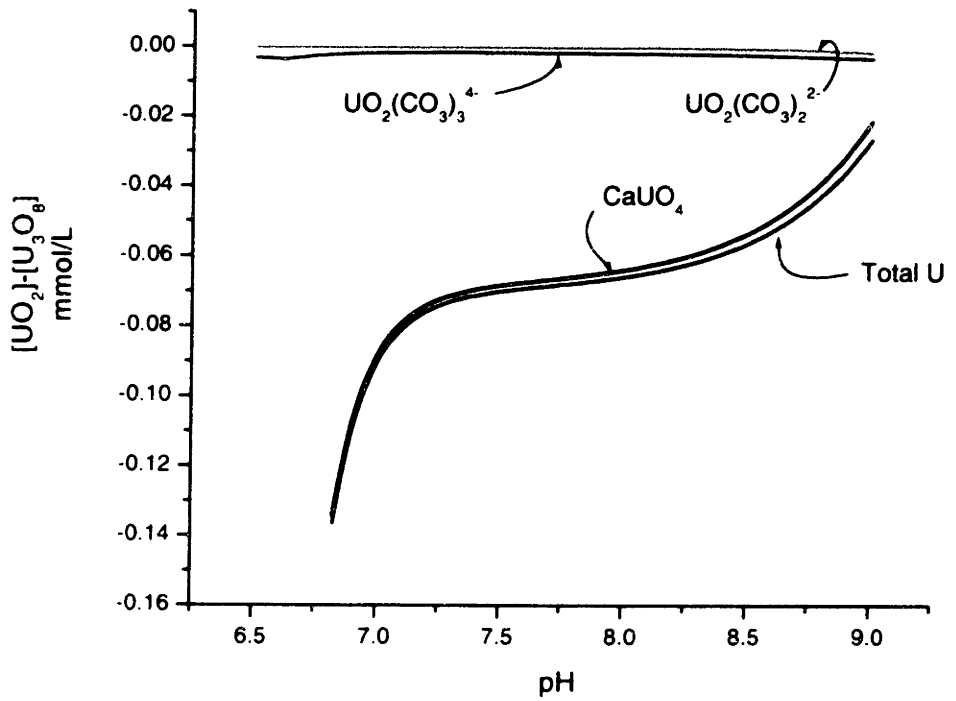

Figure E.6 [UO_2] – [U_3O_8], T = 90 °C

E.3 Conclusion

Mixed thoria-urania phase fuels will behave better in a repository environment than pure urania phase fuels due to the stabilization of the uranium phase into the less soluble UO_2 form by the thorium oxide present in the fuel. While the solubility of UO_2 is only 10% less at room temperature, it is as much as 50% lower at the predicted elevated repository temperatures. All modeling was performed under Yucca Mountain Eh and pH ranges, using water composition from nearby wells.

THESIS PROCESSING SLIP

FIXED FIELD: ill _____ name _____

index _____ biblio _____

► COPIES: Archives Aero Dewey Barker Hum

Lindgren Music Rotch Science Sche-Plough

TITLE VARIES: ► ☐ _____

_____

_____

NAME VARIES: ► ☐ _____

_____

IMPRINT: (COPYRIGHT) _____

_____

► COLLATION: _____

_____

► ADD: DEGREE: _____ ► DEPT.: _____

► ADD: DEGREE: _____ ► DEPT.: _____

SUPERVISORS: _____

_____

NOTES:

cat'r date

page

► DEPT: _____

► YEAR: _____ ► DEGREE: _____

► NAME: _____

_____